

**The Physical and Spectroscopic Study of a Series of
Poly(3-hexyl thiophene) Homopolymers and
Poly(3-hexyl thiophene)-*block*-Poly(2-hydroxyethyl
methacrylate)
Diblock Copolymers**

by

Qiliang Peng

A thesis submitted to the Department of Chemistry in conformity with the
requirements for the degree of Master of Science

Queen's University

Kingston, Ontario, Canada

March, 2010

Copyright © Qiliang Peng 2010

Abstract

In block-selective solvent, the rod-coil block copolymers can form various micellar structures. With block copolymers that contain a conjugated polymer block, the conformation of the conjugated polymer can be reflected by spectral changes in the solution. Therefore, it is of interest to study the relationship between the spectral changes and the nature of the conjugated polymer.

The fundamental physical properties of poly(3-hexyl thiophene) (P3HT) were studied. Five P3HT samples with different molecular weights were used. We have determined the relationship between physical and spectral properties of this polymer and its molecular weight. In particular, we have found that the refractive index increments, the maximum absorbance wavelength, extinction coefficients, and the emission wavelengths, increase with molecular weight.

Diblock copolymers of poly(3-hexyl thiophene)-*block*-poly(2-hydroxyethyl methacrylate) (P3HT-*b*-PHEMA) were also studied. The morphological and spectral changes of these block copolymers were studied at various stages of micelle formation in block selective solvents. The relationship between the volume fraction of the P3HT block and their physical and spectral properties were also discussed.

Acknowledgements

First of all, I would like to thank my supervisor, Prof. Guojun Liu, for his support and guidance. His inspiration and his great efforts to explain things in a clear and simple way have greatly influenced my way of thinking and approach to the scientific research. Prof. Liu has set a fantastic example not only as a scientist, but also as a successful person. His personality and thoughtfulness will affect me for a lifetime.

Special thanks are also given to my committee members, Prof. Simon A. M. Hesp and Prof. Ralph A. Whitney for offering me help and valuable suggestions.

I also want to thank Dr. Dehui Han for cooperating with me in this challenging project. Without his valuable work and strong support in the synthesis, I cannot imagine how I would navigate through this mysterious jungle of the polymer world. In addition, I wish to express my sincere gratitude to Dr. Ian W. Wyman, for always being patient while helping me solve problems.

At the same time, I would like to dedicate my grace to all of the people who worked behind the scenes: Ms. Jian Wang, Dr. De'an Xiong, Dr. Gabriel Njikang, Dr. Hongjing Dou, Dr. Jiwen Hu, Dr. Liangzhi Hong, Dr. Ronghua Zheng, Gao Yang, Hu Heng, John Dupont, Muhammad Rabnawaz, Xiaoyu Li, Zhihan Zhou, Feng Liu, Matthew Tomkins, Nan Wang, Qian Cui, and Qingxiang Song. I thank these people for giving me their friendship and encouragement over the past two years.

Last but not least, I would like to give my heartfelt thanks to my parents in China. Thank you, my Father and Mother, for your unconditional love. You have done your best to provide me with a greater education, and prayed for me from the other side of the world.

Table of Contents

Abstract	i
Acknowledgements.....	ii
Table of Contents	iv
List of Figures	viii
List of Tables.....	xi
Abbreviations.....	xii
Chapter 1. Introduction	1
1.1 Research Objectives.....	1
1.2 Organization of Thesis	2
1.3 Conjugated Polymers	3
1.4 Structure and Spectral Properties of Polythiophene	5
1.4.1 Regioregularity	5
1.4.2 Conjugation Length	7
1.4.3 Chromism.....	8
1.5 Self-Assembly of Rod-Coil Block Copolymers	11
1.5.1 Principles.....	11
1.5.2 Theories for Predicting Micellar Morphology	14
1.5.3 Main Factors Influencing on the Micellar Morphology	16

1.5.3.1 Volume Fraction of the Block.....	16
1.5.3.2 Solvent Selectivity	18
1.6 Chapter Summary	18
References.....	20
Chapter 2. Characterization of Poly(3-hexyl thiophene).....	23
2.1 Introduction.....	23
2.2 Materials and Methods.....	24
2.2.1 Synthesis	24
2.2.2 Reagents.....	27
2.2.3 Fractionation	27
2.2.4 Refractive Index Increment Measurement.....	29
2.2.5 Gel Permeation Chromatography Instrumentation	30
2.2.6 Ultraviolet-Visible Spectroscopy	30
2.2.7 Fluorescence Measurements	31
2.3 Experimental Results	32
2.3.1 Molecular Weight.....	32
2.3.2 Refractive Index Increment.....	33
2.3.3 UV-visible Spectra	34
2.3.4 Fluorescence Spectra	38
2.4 Discussion of the Properties Affected by the Molecular Weight of P3HT	40
2.4.1 Refractive Index Increment.....	40

2.4.2 Spectral Properties	41
2.4.3 Extinction Coefficient	43
2.4.4 Conjugation Length	44
2.5 Conclusions.....	46
References.....	47
Chapter 3. Morphological and Spectral Properties of Poly(3-hexyl	
thiophene)- <i>block</i> -Poly(2-hydroxyethyl methacrylate) in Various Solvents.....	48
3.1 Introduction.....	48
3.2 Materials and Methods.....	49
3.2.1 Polymer Synthesis and Characterization	49
3.2.2 Micelle Preparation.....	51
3.2.3 Transmission Electron Microscopy	52
3.2.4 Atomic Force Microscopy	53
3.2.5 Dynamic Light Scattering	53
3.2.6 Ultraviolet-Visible Spectroscopy.....	54
3.2.7 Fluorescence Spectroscopy	54
3.3 Experimental Results	55
3.3.1 Comparison of the Micellar Properties Determined by TEM, AFM, and DLS Measurements.....	55
3.3.2 UV-visible and Fluorescence Spectral Changes during Micelle Formation	61

3.4 Discussion for the Micelle Formation of the Diblock Copolymers	67
3.4.1 Factors Influencing the Sizes of Micelles	67
3.4.2 Spectral Changes of the Micellar Solutions with Varying P3HT Volume Fraction	69
3.5 Conclusions.....	73
References.....	75
Chapter 4. Summary	76
4.1 Molecular Weight Dependence of P3HT	76
4.2 Micellar Morphology of P3HT- <i>b</i> -PHEMA block copolymers	77
4.3 Significance of Work	77
4.4 Future Work	78

List of Figures

Figure 1-1	Chemical structure of P3HT.....	2
Figure 1-2	Chemical structure of P3HT- <i>b</i> -PHEMA.....	3
Figure 1-3	Chemical structure of several conjugated polymers.....	4
Figure 1-4	Four types of arrangement of P3HT triads. R above denotes an alkyl group.....	6
Figure 1-5	Conjugated π -orbitals of a substituted polythiophene in the coplanar (top) and twisted (bottom) forms.....	7
Figure 1-6	Dependence of micellar structure on the volume fraction of coil (light part) and rod (dark part) blocks.....	15
Figure 2-1	Synthesis of regioregular P3HT.....	25
Figure 2-2	¹ H NMR spectrum of P3HT.....	26
Figure 2-3	GPC plot of the five P3HT samples: T1, T2, T3, T4, T5.....	32
Figure 2-4	A typical plot of differential refractive index versus the concentration of sample T3 in the THF solution.....	33
Figure 2-5	UV-visible absorption spectra of P3HT samples in chloroform solutions.....	36
Figure 2-6	UV-visible absorption spectra of P3HT samples as thin films.....	36
Figure 2-7	Fluorescence spectra of P3HT samples in chloroform solutions.....	38
Figure 2-8	Fluorescence spectra of P3HT samples as thin films.....	38
Figure 2-9	Schematic representation of the relationship between the refractive index	

	increment of each P3HT sample in THF solution and its molecular weight.....	40
Figure 2-10	Schematic representation of the relationship between λ_{\max} and molecular weight of P3HT in chloroform solution and as a thin film.....	41
Figure 2-11	Schematic representation of the relationship between λ_{em} and the molecular weight for P3HT samples in chloroform solution and as a thin film.....	41
Figure 2-12	Schematic representation of the relationship between the extinction coefficient of each P3HT sample in chloroform solution and its molecular weight.....	43
Figure 3-1	Schematic representation of synthesis of P3HT- <i>b</i> -PHEMA.....	49
Figure 3-2	TEM image of the sample DC1 sprayed from a THF/MeOH mixture (v/v = 1/99). The sample was stained by phosphotungstic acid.....	55
Figure 3-3	TEM image of the sample DC2 sprayed from a THF/MeOH mixture (v/v = 1/99). The sample was stained by phosphotungstic acid.....	56
Figure 3-4	TEM image of the sample DC3 sprayed from a THF/MeOH mixture (v/v = 1/99). The sample was stained by phosphotungstic acid.....	56
Figure 3-5	AFM topography (left) and phase (right) images of P3HT ₃₀ - <i>b</i> -PHEMA ₈₀ sprayed from a THF/MeOH mixture (v/v = 1/99).....	58
Figure 3-6	AFM topography (left) and phase (right) images of P3HT ₄₁ - <i>b</i> -PHEMA ₈₂ sprayed from a THF/MeOH mixture (v/v = 1/99).....	58
Figure 3-7	AFM topography (left) and phase (right) images of P3HT ₅₃ - <i>b</i> -PHEMA ₆₀ sprayed from a THF/MeOH mixture (v/v = 1/99).....	59
Figure 3-8	UV-visible spectra of DC3 in different solvent mixtures, with THF/MeOH volume fractions of 94/6, 70/30, 55/45, 40/60, 20/80, and 1/99.....	62

Figure 3-9	Fluorescence spectra of DC3 in different solvent mixtures with THF/MeOH volume fractions of 94/6, 70/30, 55/45, 40/60, 20/80, and 1/99.....	62
Figure 3-10	UV-visible spectra of DC1 with increasing methanol content during the micelle formation process (THF/MeOH, v/v = 94/6, 70/30, 55/45, 40/60, 20/80, and 1/99).....	64
Figure 3-11	UV-visible spectra of DC2 with increasing methanol content during the micelle formation process (THF/MeOH, v/v = 94/6, 70/30, 55/45, 40/60, 20/80, and 1/99).....	64
Figure 3-12	Fluorescence spectra of DC1 with increasing methanol content during the micelle formation process (THF/MeOH, v/v = 94/6, 70/30, 55/45, 40/60, 20/80, and 1/99).....	65
Figure 3-13	Fluorescence spectra of DC2 with increasing methanol content during the micelle formation process (THF/MeOH, v/v = 94/6, 70/30, 55/45, 40/60, 20/80, and 1/99).....	65
Figure 3-14	Plot of the UV-visible maximum absorption wavelength (λ_{\max}) against the P3HT volume fraction before and after methanol addition.....	71
Figure 3-15	Plot of the fluorescence emission wavelength (λ_{em}) against the P3HT volume ratio before and after methanol addition.....	71
Figure 3-16	Plot of the fluorescence intensity against the methanol volume fraction, in THF/MeOH solvent mixtures during the micellar preparation process.....	72

List of Tables

Table 1-1	Typical rod block polymers	12
Table 1-2	Typical coil block polymers.....	13
Table 2-1	Fractionation results of P3HT ₄₁	28
Table 2-2	Summary of the five P3HT samples.....	31
Table 2-3	Refractive index increment of P3HT samples.....	33
Table 2-4	UV-visible spectral properties of P3HT samples.....	34
Table 2-5	Fluorescence properties of P3HT samples.....	37
Table 3-1	Summary of the diblock copolymers of P3HT- <i>b</i> -PHEMA.....	50
Table 3-2	Diameters of the micelles of P3HT- <i>b</i> -PHEMA diblock copolymers as determined by TEM, AFM, and DLS techniques.....	54
Table 3-3	Spectral properties of P3HT- <i>b</i> -PHEMA samples.....	60
Table 3-4	Comparison of the micelle diameters that were determined by TEM and AFM measurements with the calculated values.....	67

Abbreviations

AFM	atomic force microscopy
DLS	dynamic light scattering
dn/dc	refractive index increment
ε	extinction coefficient
GPC	gel permeation chromatography
λ_{\max}	maximum absorption wavelength
λ_{em}	maximum emission wavelength
MeOH	methanol
M_n	number-average molecular weight
M_w	weight-average molecular weight
NMR	nuclear magnetic resonance
P3HT	poly(3-hexyl thiophene)
PHEMA	poly(2-hydroxyethyl methacrylate)
TEM	transmission electron microscopy
THF	tetrahydrofuran
UV-visible	ultraviolet-visible light
v	volume fraction

Chapter 1. Introduction

1.1 Research Objectives

Block copolymers are composed of two or more homogeneous polymer blocks, where each block has different chemical properties, repeat unit numbers, and stiffness. When a diblock copolymer has one rigid block and one soft block, it is called a rod-coil diblock copolymer. Recently, conjugated polymers have received significant attention, because of their various applications in field-effect transistors,¹ electroluminescent devices,² solar cells,³ photochemical resists,⁴ non-linear optic devices,⁵ and chemical sensors.⁶ Conjugated polymers normally have poor solubility in most solvents. One way to introduce an insoluble conjugated polymer into other solvent systems is to prepare conjugated-polymer-containing rod-coil diblock copolymers, by connecting soluble coil polymer chains onto the conjugated block. This thesis describes a morphological and spectral study of the rod-coil diblock copolymer poly(3-hexyl thiophene)-*block*-poly(2-hydroxyethyl methacrylate) (P3HT-*b*-PHEMA), as well as the molecular characterization of the conductive polymer poly(3-hexyl thiophene) (P3HT) (Figure 1-1). The decision to study P3HT and P3HT-containing diblock copolymer in this thesis originates from the spectral change between P3HT's solvated state, and its aggregate state, which is called chromism.⁷ This property has potential for application in chromic sensors.

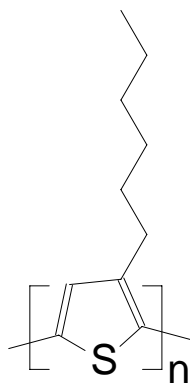


Figure 1-1. Chemical structure of P3HT.

1.2 Organization of Thesis

In this thesis, chapter 1 will briefly review the development of several common conjugated polymers, which have been widely studied in the last thirty years. Recent research of block copolymers that contain a conjugated polymer block will also be discussed. To better understand general rod-coil block copolymer systems, the theories and experimental studies of these systems will be described.

Chapter 2 will describe the properties of P3HT, which we have determined experimentally. These include the molecular weight dependence of the specific refractive index increments, as well as the absorption and emission properties of P3HT. In addition, the differences between the optical properties of the solution state and the film state of P3HT will be discussed.

Chapter 3 will focus on the morphology and spectral change of the aggregates of P3HT-*b*-PHEMA in solvents. Three different P3HT-*b*-PHEMA polymer samples were prepared, with different unit lengths, in order to demonstrate the effect of the different

block length on their spectral properties. These investigations were conducted by transmission electron microscopy, atomic force microscopy, and dynamic light scattering. The mechanism of self-assembly of the P3HT-*b*-PHEMA will also be proposed.

Chapter 4 will draw conclusions based on the work presented, and will outline some areas where the study of the block copolymer P3HT-*b*-PHEMA may be applied.

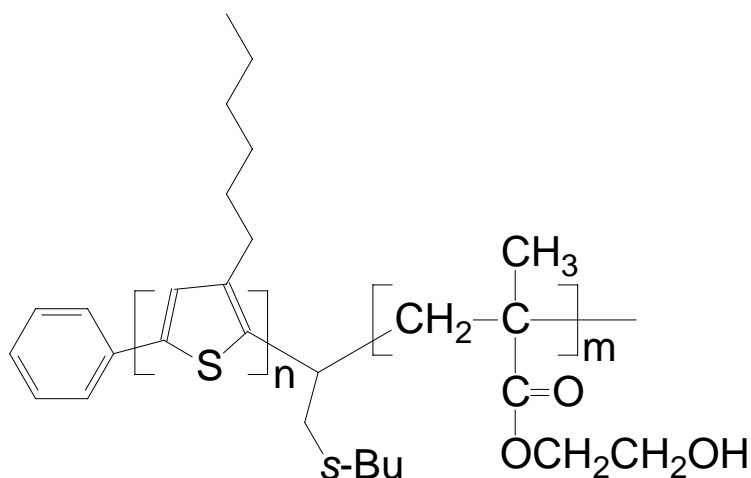


Figure 1-2. Chemical structure of P3HT-*b*-PHEMA.

1.3 Conjugated Polymers

The most widely studied conjugated polymers are shown in Figure 1-3. Certain conjugated polymers, which behave as electrical semiconductors, are sometimes called conductive polymers. Their conductivity can be as high as 10^5 S/cm,^{6,8} while the polymers prepared from the polymerization of vinyl monomers are normally used as insulators. According to their unique electronic, mechanic, and processing characteristics, conductive polymers have been considered as candidates for applications which have traditionally been fulfilled by metals and semiconductors.

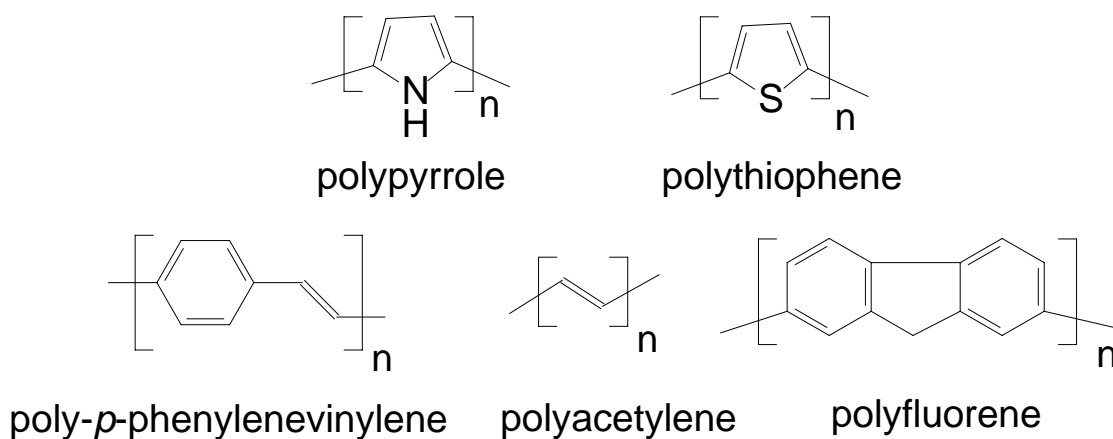


Figure 1-3. Chemical structure of several conjugated polymers.

In the early 1900s, German chemists had reported polypyrrole, then known as “pyrrole black”.⁹ However, its electrical conductivity and π -conjugation structure were not realized at that time. In 1977, Alan J. Heeger, Alan MacDiarmid, and Hideki Shirakawa reported the discovery of the conductive properties of doped polyacetylene, one of the first known examples of a conductive organic polymer.^{10,11} Polyacetylene has the simplest structure of the conductive polymers presented in Figure 1-3 with the repeat unit $(C_2H_2)_n$ completely in either the *cis* or *trans* configuration, and does not dissolve in organic solvents. When doped with iodine, bromine, boron trifluoride (BF_3), or arsenic trifluoride (AsF_3), the conductivity of this polymer approaches that of metals.¹² Due to their extensive research in the semiconducting and conducting properties of several polyacetylene-series conjugated polymers, Heeger, MacDiarmid, and Shirakawa received the Nobel Prize in Chemistry in 2000.

Moreover, the discovery of the conductive properties of polyacetylene resulted in the rapid development of polymer based electrical components, such as polymeric light

emitting diodes,² and organic solar cells,³ where poly(*p*-phenylene vinylene) (PPV), polyfluorene (PF), and poly(3-hexyl thiophene) (P3HT) are now widely used. PPV, a red metallic polymer, is capable of electroluminescence, and was often used as the emissive layer, such as in the first polymer light-emitting diodes.¹³ In general, PPV-based devices can emit a yellowish-green light, and emissions of different wavelengths can be obtained by changing the substituted functional groups on the aryl ring. In a similar manner to that of PPV, upon excitation the emitted light from PF can cover the entire visible spectrum⁴ by tuning the functional group grafted onto the fluorene unit.^{14,15}

P3HT is the most widely studied polythiophene (Figure 1-1). The hexyl group can increase the polymer's solubility to the point where it is suitable for applications in flexible electronic devices, such as printed integrated circuits, and printed photovoltaic panels.^{3,16,17}

1.4 Structure and Spectral Properties of Polythiophene

1.4.1 Regioregularity

Regioregularity refers to the symmetry in the linkage of the 3-substituted thiophene units. Two monomers can be linked *via* their 2- and 5-positions. This is referred to as 2,5', or head-to-tail (HT) coupling. Analogously, they can be linked through their 2,2' positions, to give head-to-head (HH) coupling, or through their 5,5' positions, to give

tail-to-tail (TT) coupling. For triads, four possible structures are possible through the different combinations of the diads that could exist in the P3HT chains (shown in Figure 1-4).

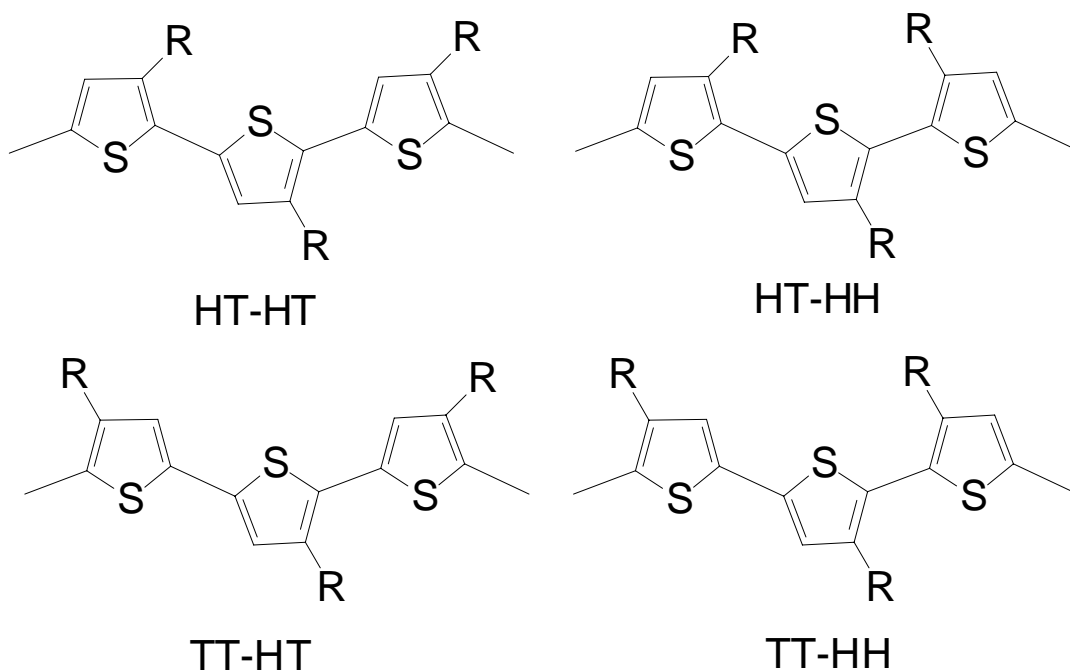


Figure 1-4. Four types of arrangement of P3HT triads. R above denotes an alkyl group.

Through ^1H NMR spectroscopy, the regioregularity of a sample of P3HT can be determined.⁶ The signal at 6.98 ppm, which is located in the aromatic portion of the ^1H NMR spectrum, is ascribed to the HT-HT triad. Singlet peaks, corresponding to regioregularity defects attributed to the HT-HH, TT-HT, and TT-HH structures, would appear at 7.00, 7.02, and 7.05 ppm, respectively. The regioregularity of P3HT can be determined by calculating the proportion of the integral representing the HT-HT triad with respect to the four possible types of triad arrangements.

1.4.2 Conjugation Length

The conjugation length is a reflection of the number of coplanar thiophene rings. A longer conjugation length corresponds to a smaller separation between the highest occupied molecular orbital (HOMO) and the lowest unoccupied molecular orbital (LUMO) energy levels, and also longer absorption wavelengths. In other words, coplanarity of the conjugated polythiophene can allow the π -electrons to become delocalized along the polymer backbone. However, deviations from coplanarity may occur, resulting from defects of the linkages between the monomers during the synthesis, or also from steric hindrance of bulky side-chains. Deviations from coplanarity can also be caused by external stimuli, such as the solvent,¹⁸ temperature,¹⁹ and ionic strength.²⁰ These deviations can lead to polythiophene chain twisting, which cause the separations between π -electron energy levels to increase. Thus the conjugation length is reduced (Figure 1-6), which is reflected by a shorter absorption wavelength.

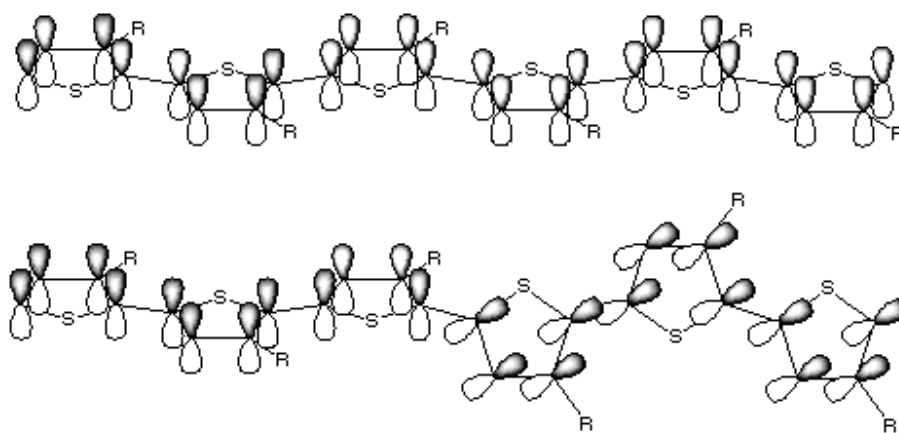


Figure 1-5. Conjugated π -orbitals of a substituted polythiophene in the coplanar (top) and twisted (bottom) forms.²¹

The maximum effective conjugation length is that above which the absorption spectrum of P3HT does not undergo further red shifts.²² Experimentally, the absorption band in the visible region is increasingly red-shifted as the number of repeat units of the polymer increases. Early studies by Hoeve *et al.* estimated that the effective conjugation of a thiophene derivative was extended over 11 repeat units,²³ while later studies increased this estimate to 20 units.²⁴ More recently, Otsubo *et al.* synthesized a series of polythiophenes from 6 units to 96 units.²⁵ They found a 0.1 nm difference in the red shift between the 72- and the 96-units polythiophenes, indicating that the effective conjugation length may be even longer than 96 units.

1.4.3 Chromism

Generally speaking, chromism refers to the phenomenon of reversible color change of a material that is subjected to the external stimuli, such as heat, solvent polarity change, addition of ions, or complexation with other compounds.^{18,26} The most common chromism phenomenon observed is solvatochromism, which refers to a color change between the solid and solvated state of a conjugated polymer. The driving force of solvatochromism originates from the interaction between the polymer chain and the solvent, based on their polarity difference. Poly(3-alkylthiophene)s (P3AT) are known to be solvatochromic. As the P3AT chain precipitates from solution, it changes its conformation from a twisted to a folded morphology, and its color changes from yellow to purple.^{27,28} Studies on the polythiophene aggregation process attributed the spectral

change either to intermolecular coplanarization aggregation,²⁹ or to an intramolecular backbone conformation transition.³⁰⁻³³ In other words, P3HT interchain π - π stacking interactions, and intrachain coplanarization of the thiophene units will occur in the presence of a poor solvent. As a result, a decrease in the band gap is observed, as reflected by a red shift in the UV-visible absorption spectra.

Thermochromism is a phenomenon which describes reversible spectral shifts generated by a temperature change. This can also be associated with conformation changes of a polymer's backbone.¹⁹ Due to the thermal motion, increasing temperature has a similar effect as decreasing the solvent polarity, and vice-versa. The absorption peak shift results from a conformational transition from a coplanar, rod-like phase at lower temperatures, to a twisted, coil-like phase at elevated temperatures. One interesting aspect of the thermochromism study of polythiophene derivatives is the isosbestic point, which is a point at which the absorbance spectra overlap. The presence of an isosbestic point indicates the coexistence of two conformations of P3HT, the coplanar one and the twisted one. Roux and Leclerc reported that poly(3-(octyloxy)-4-methylthiophene)'s violet color (550 nm) at 25 °C changes to a yellowish orange color (390 nm) at 150 °C, and has an isosbestic point at 450 nm.¹⁹ However, not all thermochromic polythiophenes exhibit an isosbestic point. Tachibana *et al.*³⁴ studied the thermochromism of regioregular poly(3-alkylthiophene) with different length alkyl groups lengths (C_nH_{2n+1} , $n = 4, 8, 14, 20$). Only poly(3-butylthiophene) displayed a continuous blue-shift with increasing temperature. This indicated that upon

melting, the chains of poly(3-butylthiophene) do not interconvert between crystalline and amorphous phases at low temperatures, due to its greater coplanar chain packing order compared to the other polymers in this study.

Another type of reversible color change for molecules in solution is called ionochromism, and is caused by the addition of ions.³⁵ These ions can trigger the alteration of a material's micromorphology, along with the spectral change. Ionochromic effects were initially reported for regioregular polythiophenes with grafted crown ether side chains.³⁶ These polymers can undergo conformational changes upon coordination with alkali-metal ions, such as lithium, sodium, and potassium, creating interesting sensory systems.³⁷ These conformational changes are dependent on the size of the ions, and their binding strength with the host material. Leclerc *et al.* studied the ionochromic properties of regioregular polythiophene with pendant oligo(ethyleneoxide) chains.^{38,39} They found that noncovalent interactions between ether-substituted regioregular polythiophenes and ionic species can be used to stabilize the coplanar form of the backbone. In addition to metal ions, acid/base chromic systems are controlled by the adjustment of the pH value of the solution. The research done by Winnik and co-workers shows that the polythiophene-*graft*-poly(*N,N*-dimethylaminoethyl methacrylate) (PT-*g*-PDMA),⁴⁰ changes color from the yellow to the orange, when the pH is gradually decreased from 8 to 2. In this process, the amino groups on the polymer will be protonated. The increasing repulsive interaction within the cationic PDMA block drives the absorption and fluorescence spectral shift of the polythiophene backbone

chain. Due to the hydrophilic nature of the PDMA block, this block copolymer is soluble in aqueous solutions. This aqueous solubility may allow potential applications as the biosensor to detect the pH change from the spectral change of polythiophene group.⁴¹

1.5 Self-Assembly of Rod-Coil Block Copolymers

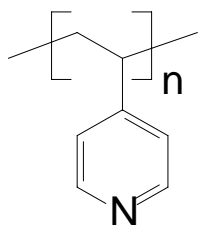
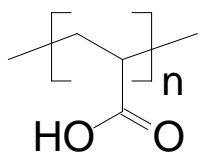
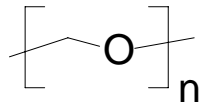
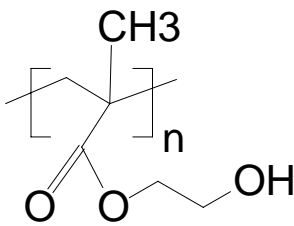
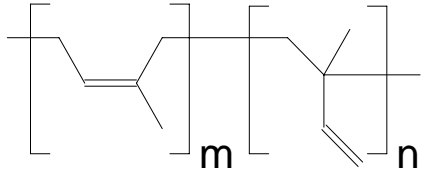
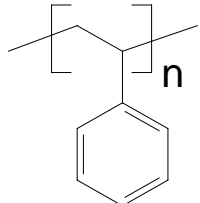
1.5.1 Principles

Rod-coil block copolymers consist of rigid, rod-like blocks and flexible, coil-like blocks in the same molecule. The rigidity of a polymer is described by its persistence length, which is the projected end-to-end distance with respect to the vector of the first unit of a polymer backbone. For a perfectly rigid chain with infinite length, the persistence length is infinite, while for a perfectly flexible chain, the persistence length is zero. Tables 1-1 and 1-2 list some typical rod and coil polymers, respectively. For some examples, rigid P3HT has a persistence length of 2.4 nm,³² while flexible poly(ethylene oxide) and polystyrene have persistence lengths of 3.7 and 9.0 Å, respectively.^{42,43} Therefore, compared to flexible polymers, P3HT is normally referred to as a rod-like polymer, because of its π -conjugated structure, and rigid thiophene ring unit, which increases the rigidity of the polymer.

Table 1-1. Typical rod block polymers.

Polymer Name	Acronym	Chemical Structure
Poly(3-hexyl thiophene)	P3HT	
Polyfluorene	PF	
Polyisocyanate	PIC	
Poly(L-glutamic acid)	PLGA	
Poly(paraphenylene)	PPP	
Poly(phenylquinoline)	PPQ	
Poly(p-phenylene vinylene)	PPV	

Table 1-2. Typical coil block polymers.

Polymer Name	Acronym	Chemical Structure
Poly(4-vinylpyridine)	P4VP	
Poly(acrylic acid)	PAA	
Poly(ethylene oxide)	PEO	
Poly(2-hydroxyethyl methacrylate)	PHEMA	
Polyisoprene	PI	
Polystyrene	PS	

Block copolymers can be used to form micelles with controlled sizes and shapes in selective solvents, which act as good solvents for one block, and poor solvents for the other block.⁴⁴ The micelles described in this thesis have the core/corona structures, with the core and corona formed by the rod and coil blocks, respectively. The differences in chain rigidity between the rod and the coil blocks are expected to greatly affect the properties of copolymer molecular packing in the micellar aggregates.⁴⁵⁻⁴⁹ Also, the entropic penalty associated with the chain stretching of the rod blocks, and the interfacial energy between the micelle and the solvent, will result in the self-assembly of block copolymers into a variety of micellar structures.^{50,51}

1.5.2 Theories for Predicting Micellar Morphology

One simple way to estimate the micellar morphology of the diblock copolymer is to check the packing parameter, p :

$$p = V/(A \cdot R)$$

where V is the volume of the insoluble block, A is the surface area of the soluble head block at the critical micelle concentration, and R is the radius of the micellar core.⁵² An approximate estimation for the micellar morphology given in Figure 1-7 would be:

For spheres,
$$p = \frac{4}{3}\pi r^3 / 4\pi r^2 \cdot r = \frac{1}{3}$$

For cylinders,
$$p = \pi r^2 l / 2\pi r l \cdot r = \frac{1}{2}$$

For disklike micelles,
$$p = Ar / A \cdot r = 1$$

Lee and co-workers applied this packing parameter concept toward designing

conjugated rod-coils PPP-*b*-PEO.^{53,54} The molecular design was implemented by varying either the PEO coil length or the PPP rod repeat unit number. From this molecular design approach, they were able to tune the size and shape of the micellar nanostructures, from spheres to vesicles and cylinders.

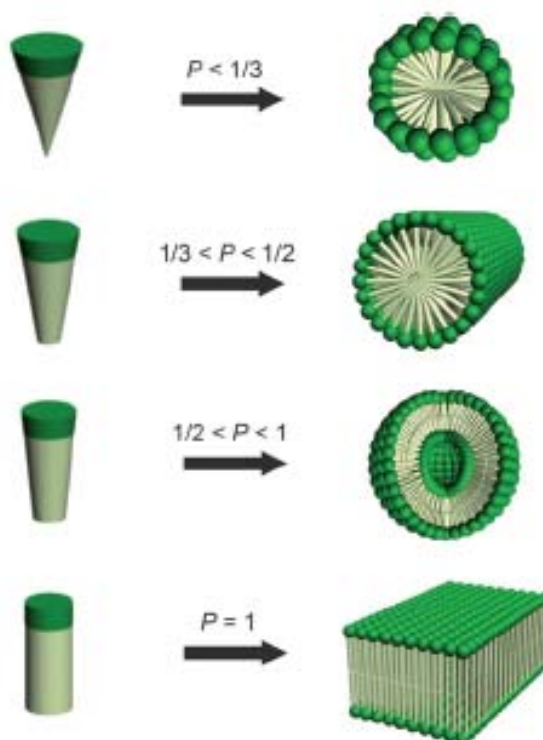


Figure 1-6. Dependence of micellar structure on the volume fraction of coil (dark part) and rod (light part) blocks.⁵⁵

However, there are a large number of factors influencing the rod-coil block copolymer micelle formation, such as, volume fraction of the block, solvent selectivity, π - π interaction, concentration, structural difference, and thermal processing history. It is very difficult to explain the various cases with such a simple model. Several theoretical models have been developed to help better understand the formation of the solution

self-assembly structures of coil-rod block copolymers. Horsch *et al.* performed Brownian dynamic simulations of rod-coil block copolymers in a coil-selective solvent, while eliminating interactions between the rods.^{56,57} Their simulations predicted cylindrical micelles as the stable self-assembled nanostructures, with changing the concentration and the coil fraction. Fredrickson proposed the hockey-puck-like micelle, where the rods are packed axially to form finite-sized cylindrical disks covered by coils.⁵⁸ They predicted that the hockey puck structure should be stable at large (> 0.9) coil fractions. The main advantage of micelle formation relative to the lamellae structure is the reduction of the stretching penalty of coils, because the complete separation is impossible due to the coils permanent attachment to the rod blocks.

1.5.3 Main Factors Influencing on the Micellar Morphology

1.5.3.1 Volume Fraction of the Block

The volume fraction of the block (or the relative volume fraction) of the rod block affects morphology of micelles formed from a rod-coil diblock copolymer. For example, poly(ethylene oxide)-*block*-poly(*p*-benzamide) (PEO-*b*-PPBz) forms spherical micelles in chloroform for copolymers with a long soluble PEO coil block, for example, at 110 repeat units.⁵⁹ Meanwhile, puck-like bilayer micelles of PEO-*b*-PPBz with short PEO blocks, such as 45 repeat units, can be obtained if the length of the PPBz block is kept below 60 repeat units.⁵⁹ Kim and co-workers^{53,54} also investigated mesogenic rods

linked to PEO coils of varying molecular weight, finding that vesicular micelles were formed for short PEO coils (12 repeat units), while spherical micelles were formed for longer coils (23 repeat units). Surin *et al.*⁶⁰ applied tapping-mode atomic force microscopy to investigate the relationship between the molecular structure and the microscopic morphology of polyfluorene-*block*-poly(ethylene oxide) (PF-*b*-PEO). Their results showed that copolymers with a low PEO coil volume fraction ($v_{\text{PEO}} = 0.1 \sim 0.3$) exhibit well-defined nanoribbon structures, while at higher volume fractions ($v_{\text{PEO}} > 0.4$), the organized structures disappear and lead to disordered aggregates. This phenomenon is probably due to the lack of the long-range and regular π - π stacking of the PF segments.⁶¹

Moreover, changing the length of the rod block in a coil-selective solvent will also alter the micellar morphology. Mori and co-workers⁶² found that the micelles of poly(dioctyloxyphenylenevinylene)-*block*-poly(ethylene oxide) (PDOOPV-*b*-PEO) in THF/water mixtures had a transition from the cylinders ($v_{\text{ppv}} = 0.046$) to the spheres ($v_{\text{ppv}} = 0.20$). The shape of the aggregates was insensitive to solvent composition and polymer concentration. Poly(*p*-phenylene)-*block*-polystyrene (PPP-*b*-PS) block copolymers were found to have the similar transition phenomenon.^{63,64} When it forms spherical micelles in coil-selective THF/trichlorobenzene solutions, the size of the micellar core is independent of polymer concentration, but increases steadily with increasing length of the PPP block. This indicates that the core sizes in the discussion above are determined primarily by the length of the rod block.

1.5.3.2 Solvent Selectivity

Solvent selectivity has an impact on the morphology of rod-coil diblock copolymer micelles. Increasing the solvent selectivity for the coil block leads to a series of transitions, from aggregated spherical micelles, to individual spherical micelles, and to vesicles. Studies by Tung *et al.* regarding polyfluorene-*block*-poly(acrylic acid) (PF-*b*-PAA) have revealed the relationship between the micellar morphology and solvent selectivity.⁶⁵ They showed that decreasing solvent quality for the rod block of the PF-*b*-PAA results in the transition from spheres to vesicles. On the other hand, decreasing solvent quality for the coil block of the PF-*b*-PAA resulted in an inversion process, which was from vesicles and nanorods were formed with further decreasing solvent quality. It appears that this inversion is driven by the alignment of the PF blocks as they pack at the micellar core. A similar phenomenon was observed in a triblock system of polystyrene-*block*-poly(phenylene vinylene)-*block*-polystyrene (PS-*b*-PPV-*b*-PS), which was prepared in toluene/methanol and trichloroethane/methanol mixtures.⁶⁶ Thus it suggests that solvent selectivity can be used to control the morphology of the rod-coil diblock copolymer micelles.

1.6 Chapter Summary

In this chapter, two areas have been reviewed, including conjugated polymers and the self-assembly of rod-coil block copolymers. Several kinds of common conjugated

polymers were shown. This was followed by a closer examination of three specific properties of P3HT, including regioregularity, conjugation length, and chromism. Secondly, the principles, theories, and factors that may influence the micellar morphology of rod-coil diblock copolymers were also discussed. A number of published experimental results have been cited to help explain these key concepts.

References

- 1 Garnier, F. Field-Effect Transistors Based on Conjugated Materials. In *Electronic Materials: The Oligomer Approach*; Müllen, K., Wegner, G., Eds.; Wiley-VCH, Weinheim, 1998, pp.1-7.
- 2 McCullough, R. D. *Adv. Mater.* **1998**, *10*, 93-116
- 3 Yu, G.; Gao, J.; Hummelen, J. C.; Wudl, F.; Heeger, A. J. *Science* **1995**, *270*, 1789
- 4 Leclerc, M. *J. Polym. Sci. Part A : Polym. Chem.* **2001**, *39*, 2867-2873
- 5 Harrison, M. G.; Friend, R. H. Optical Applications. In *Electronic Materials: The Oligomer Approach*, Müllen, K., Wegner, G., Eds.; Wiley-VCH, Weinheim, 1998, pp. 1-9.
- 6 Trznadel, M.; Pron, A.; Zagorska, M.; Chrzaszcz, R.; Pielichowski, J. *Macromolecules* **1998**, *31*, 5051-5058.
- 7 Chen, S. A.; Ni, J. M. *Macromolecules* **1992**, *25*, 6081-6089.
- 8 Boggild, P.; Grey, F.; Hassenkam, T.; Greve, D. R.; Bjornholm, T.; *Adv. Mater.* **2000**, *12*, 947-950.
- 9 Tsukamoto, J.; *Adv. Phys.* **1992**, *41*, 509.
- 10 Inzelt, G., Scholz, F., Eds.; Monographs in Electrochemistry; *Conducting Polymers*; Springer-Verlag; Berlin Heidelberg, Germany, 2008, pp. 1-8.
- 11 Chiang, C. K.; Druy, M. A.; Gau, S. C.; Heeger, A. G.; Louis, E. J.; MacDiarmid, A. G.; Park, Y. W.; Shirakawa, H. *J. Am. Chem. Soc.* **1978**, *100*, 1013-1017
- 12 Heeger, A. J.; Kivelson, S.; Schrieffer, J. R.; Su, W. P. *Rev. Modern Phys.* **1988**, *60*, 781-785.
- 13 Burroughes, J. H.; Bradley, D. D. C.; Brown, A. R.; Marks, R. N.; Mackay, K.; Friend, R. H.; Burn, P. L.; Holmes, A. B. *Nature* **1990**, *347*, 539.
- 14 Grell, M.; Bradley, D. D. C.; Long, X.; Chamberlain, T.; Inbasekaran, M.; Woo, E. P.; Soliman, M. *Acta Polym.* **1998**, *49*.
- 15 Gu, H. B.; Morita, S.; Yin, X. H.; Kawai, T.; Yoshino, K. *Synth. Met.* **1995**, *69*, 449.
- 16 Sariciftci, N. S.; Smilowitz, L.; Heeger, A. J.; Wudl, F. *Science* **1992**, *258*, 1474.
- 17 Yu, G.; Heeger, A. J. *J. Appl. Phys.* **1995**, *78*, 4510.
- 18 Okada, S.; Peng, S.; Spevak, W.; Charych, D. *Acc. Chem. Res.* **1998**, *31*, 229-239.
- 19 Wacharasindhu, S.; Montha, S.; Boonyiseng, J.; Potisatityuenyong, A.; Phollookin, C.; Tumcharern, G.; Sukwattanasinitt, M.. *Macromolecules* **2010**, *43*, 716-724.
- 20 McQuade, D. T.; Pullen, A. E.; Swager, T. M. *Chem. Rev.* **2000**, *100*, 2537-2574.
- 21 File:Polythiophenes Conjugation.png.
http://en.wikipedia.org/wiki/File:Polythiophenes_Conjugation.png (accessed June 2009)

- 22 Ho, K.-S.; Huang, Y.-J.; Kuo, C.-W.; Lee, S.-W.; Hsieh, T.-H.; Chuang, C.-N. *J. Appl. Polymer Sci.* **2007**, *103*, 2120-2128.
- 23 Hoeve, W.; Wynberg, H.; Havinga, E. E.; Meijer, E. W. *J. Am. Chem. Soc.* **1991**, *113*, 5887-5889.
- 24 Meier, H.; Stalmach, U.; Kolshorn, H. *Acta Polymerica* **1997**, *48*, 379-384.
- 25 Izumi, T.; Kobashi, S.; Takimiya, K.; Aso, Y.; Otsubo, T. *J. Am. Chem. Soc.* **2003**, *125*, 5286-5287.
- 26 Bässler, H. Electronic Excitation. In *Electronic Materials: The Oligomer Approach*; Müllen, K.; Wegner, G., Eds.; Wiley-VCH: Weinheim, Germany 1998.
- 27 Ihn, K.; Moulton, J.; Smith, P. *J. Polym. Sci. Part B, Polym. Phys.* **1993**, *31*, 735.
- 28 Mardelen, J.; Samuelsen, E.; Pendersen, A.; *Synth. Met.* **1993**, *55*, 378.
- 29 Rughooputh, S. D. D. V.; Hotta, S.; Heeger, A. J.; Wudl, F. *J. Polym. Sci., Part B: Polym. Phys.* **1987**, *25*, 1071-1074.
- 30 Chen, S. A.; Ni, J. M. *Macromolecules* **1992**, *25*, 6081-6089.
- 31 Daoust, G.; Leclerc, M. *Macromolecules* **1991**, *24*, 455-459.
- 32 Heffner, G. W.; Pearson, D. S. *Macromolecules* **1991**, *24*, 6295- 6299.
- 33 Roux, C.; Leclerc, M. *Macromolecules* **1992**, *25*, 2141-2144.
- 34 Tachibana, H.; Hosaka, N.; Tokura, Y. *Macromolecules* **2001**, *34*, 1823-1827.
- 35 Yuan, Z.; Lee, C.-W.; Lee, S.-H. *Polymer* **2005**, *46*, 3564-3566.
- 36 McQuade, D. T.; Pullen, A. E.; Swager, T. M. *Chem. Rev.* **2000**, *100*, 2537-2574.
- 37 Levesque, I.; Leclerc, M. *J. Chem. Soc., Chem. Commun.* **1995**, 2293-2294.
- 38 Faid, K.; Frechette, M.; Ranger, M.; Mazerolle, L.; Levesque, I.; Leclerc, M.; Chen, T.-A.; Rieke, R. D. *Chem. Mater.* **1995**, *7*, 1390-1396.
- 39 Levesque, I.; Leclerc, M. *Chem. Mater.* **1996**, *8*, 2843-2849.
- 40 Wang, M.; Zou, S.; Guerin, G.; Shen, L.; Deng, K.; Jones, K.; Walker, G. C.; Scholes, G. D.; Winnik, M. A. *Macromolecules* **2008**, *41*, 6993-7002.
- 41 Ho, H.-A.; Najari, A.; Leclerc, M. *Acc. Chem. Res.* **2008**, *41*, 168-178.
- 42 Lee, H.; Venable, R. M.; Mackerell, A. D.; Pastor, R. W. *Biophys. J.* **2008**, *95*, 1590-1599.
- 43 Wignall, G. D.; Ballard, D. G. H.; Schelten, J. *Eur. Polym. J.* **1974**, *10*, 861.
- 44 Mathews, C. K.; van Holde, K. E.; Ahern, K. G. Ionic Equilibria. In *Biochemistry* 3rd Ed. Addison Wesley Longman. 1999, San Francisco, p. 38.
- 45 Lim, Y.-B. Lee E.; Lee, M. *Angew. Chem., Int. Ed.*, **2007**, *46*, 9011.
- 46 Radzilowski, L. H.; Wu J. L.; Stupp, S. I.; *Macromolecules*, **1993**, *26*, 879.
- 47 Klok, H.-A. Langenwalter J. F.; Lecommandoux, S. *Macromolecules*, **2000**, *33*, 7819.
- 48 Chen, J.-Z.; Zhang, C.-X. Sun, Z.-Y. An L.-J. Tong, Z. *J. Chem. Phys.*, **2007**, *127*, 024105.
- 49 Singh, C. Goulian, M. Liu A. J.; Fredrickson, G. H. *Macromolecules*, **1994**, *27*, 2974.
- 50 Williams D. R. M.; Fredrickson, G. H. *Macromolecules*, **1992**, *25*, 3561.

- 51 Semenov, A. N. *Mol. Cryst. Liq. Cryst.*, **1991**, *209*, 191.
- 52 Israelachvili, J. N. *Intermolecular and Surface Forces*, Academic Press, New York, 1985, pp. 1-10.
- 53 Kim, B.-S. Yang, W.-Y. Ryu, J.-H. Yoo Y.-S. Lee, M. *Chem. Commun.* **2005**, 2035.
- 54 Kim, B.-S. Hong, D.-J. Bae J. Lee, M. *J. Am. Chem. Soc.*, **2005**, *127*, 16333.
- 55 Lim, Y.-B.; Moon, K.-S.; Lee, M. *J. Mater. Chem.*, **2008**, *18*, 2909-2918.
- 56 Horsch, M. A.; Zhang, Z. L.; Glotzer, S. C. *J. Chem. Phys.* **2006**, *125*, 184903-1-12.
- 57 Horsch, M. A.; Zhang, Z. L.; Glotzer, S. C. *Phys. Rev. Lett.* **2005**, *95*, 056105-1-4.
- 58 Williams, D. R. M.; Fredrickson, G. H. *Macromolecules* **1992**, *25*, 3561.
- 59 Schleuss, T. W.; Abbel, R.; Gross, M.; Schollmeyer, D.; Frey, H.; Maskos, M.; Berger, R.; Kilbinger, A.F.M. *Angew. Chem. Inter. Ed.* **2006**, *45*, 2969-2975.
- 60 Surin, M.; Marsitzky, D.; Grimsdale, A. C.; Mullen, K.; Lazzaroni, R.; Leclere, P. *Adv. Funct. Mater.* **2004**, *14*, 708-715.
- 61 Zhang, Z. J.; Qiang, L. L. Liu, B. Xiao, X. Q.; Wei, W.; Peng, B. Huang, W. *Mater. Lett.* **2006**, *60*, 679-684.
- 62 Mori, T.; Watanabe, T.; Minagawa, K.; Tanaka, M. *J. Polym. Sci. Part A: Polymer Chemistry* **2005** *43*, 1569-1578.
- 63 Zhong, X.F.; Francois, B. *Synth. Met.* **1989**, *29*, 35-40.
- 64 Francois, B.; Widawski, G.; Rawiso, M.; Cesar, B.; *Synth. Met.* **1995**, *69*, 463-466.
- 65 Tung, Y.-C.; Wu, W.-C.; Chen, W.-C.; *Macromol. Rapid Comm.* **2006**, *27*, 1838-1844.
- 66 Li, K.; Guo, H.; Liang, Z.-Q.; Thiyagarajan, P.; Wang, Q.-J. *Polym Sci. Part A: Polymer Chemistry* **2005**, *43*, 6007-6019.

Chapter 2. Characterization of Poly(3-hexyl thiophene)

2.1 Introduction

The molecular weight of a polymer can influence its physical properties, including optical, dielectric, thermal, and mechanical properties. A polymer's molecular weight is related to its chain length, and also correlates with the end-to-end distance, hydrodynamic radius, intrinsic viscosity, and polymer conformation. Thus, by studying the relationship between the molecular weight of a polymer and its physical properties, one can reveal basic information of the physical conformation of the polymer. For example, Kline *et al.* reported that the charge transport mobility of field-effect transistors that were made from poly(3-hexyl thiophene) (P3HT) were enhanced with increasing molecular weight.¹ Brinkmann and Rannou applied high-resolution transmission electron microscopy (HR-TEM) techniques to study P3HT.² They discovered that a 10-fold increase in molecular weight from 7.3×10^3 to 6.93×10^4 g/mol leads to an enhanced interconnectivity between crystalline lamellae through tie-like crystallites.

The accuracy of interpretations about the relationship between the molecular weight of P3HT and its spectral properties depend on several parameters. The first factor is whether the polymer has a low polydispersity index, or a narrow molecular weight distribution. Secondly, P3HT must have high regioregularity, since a regular chain microstructure promotes ordered chain packing and charge transport in the solid films.³

The P3HT polymers used in previous studies had either high polydispersity indices and/or low regioregularity.^{2,4-7} In this project, I have studied the relationship between the spectroscopic properties of P3HT and its molecular weight, using P3HT samples that had both low polydispersities and high regioregularities. These spectroscopic properties include the molar extinction coefficient, the absorption and emission maxima, as well as specific refractive index increments.

2.2 Materials and Methods

2.2.1 Synthesis

Vinyl-terminated poly(3-hexyl thiophene) were prepared by utilizing a modified Grignard metathesis reaction procedure, as described previously by Jeffries-El *et al.*⁸ These polymers were synthesized by Dr. Dehui Han of our research group. The reactions used for the preparation of vinyl-terminated P3HT are shown in Figure 2-1.

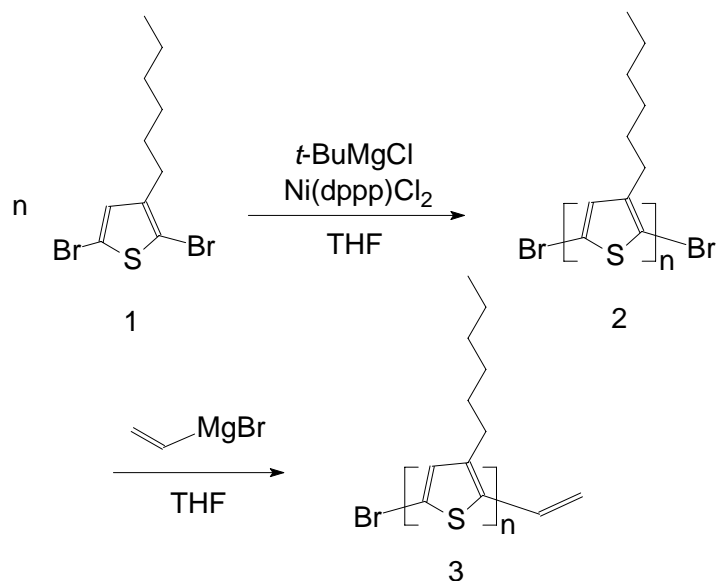


Figure 2-1. Synthesis of regioregular P3HT.

The polymerization was performed in a flamed-dried 1000 mL three-necked round bottom flask containing a Teflon-coated magnetic stir bar under nitrogen. Initially, 2,5-dibromo-3-hexyl thiophene (Compound (1), 24.45 g, 75 mmol) and freshly distilled THF (150 mL) were added into the flask. A THF solution of *tert*-butyl magnesium chloride ($t\text{-BuMgCl}$, 1.0 M, 75 mL) was transferred into the flask with a syringe. The mixture was allowed to react for 3 h at room temperature before dilution by 750 mL of dry THF. This was followed by the addition of 1,3-bis(diphenylphosphino)propane nickel-(II) chloride (Ni(dppp)Cl_2 , 0.474 g, 0.87 mmol) in one portion. The polymerization of P3HT (2) was allowed to proceed for 15 min at room temperature. Subsequently, vinyl magnesium bromide (1.0 M THF solution, 25 mL, 25 mmol) was added and the reaction was continued for 5 min in order to facilitate the vinyl end group functionalization. This reaction mixture was poured

into methanol in order to precipitate the vinyl-terminated P3HT (**3**). This crude polymer was then collected by centrifugation. After this polymer was re-dissolved into THF, it was further purified by three repeated precipitations from methanol. The P3HT samples were subsequently characterized by ^1H NMR spectroscopy.

From the ^1H NMR data it would be possible to calculate the regioregularities and the numbers of repeat units of the P3HT samples. The number of repeat units could be determined by comparing the relative integrals corresponding to protons of the polymer chain with those corresponding to the end groups. As an example, the number of repeat units could be determined by dividing the integral corresponding to protons *g* (I_g) in Figure 2-2 by the integrals of either protons *i* or *j* (I_i or I_j , respectively). As an example, the number of repeat units could thus be determined by the ratio of I_g/I_i or I_g/I_j . In a similar manner, the number of repeat units could be determined from the relative integral of protons *a* (I_a) within the polymer chain compared to protons *i* or *j*. This could be calculated as $I_a/2I_i$, $I_a/2I_j$, or $I_a/(I_i+I_j)$.

The regioregularities of the P3HT samples could also be determined based on the integrals from ^1H NMR. For example, the regioregularity of the polymers could be calculated based on the relative integrals corresponding to peak *a* (I_a), which are in the Head-to-Tail-Head-to-Tail (HT-HT) arrangement, compared to the total of the peaks corresponding to *a*, *a'*, and *a''* of Figure 2-2. Meanwhile, the regioregularity could also be calculated from the ratio of the integral of peak *g* (I_g) compared to the total integral of the peaks corresponding to *g*, *g'*, and *g''*.

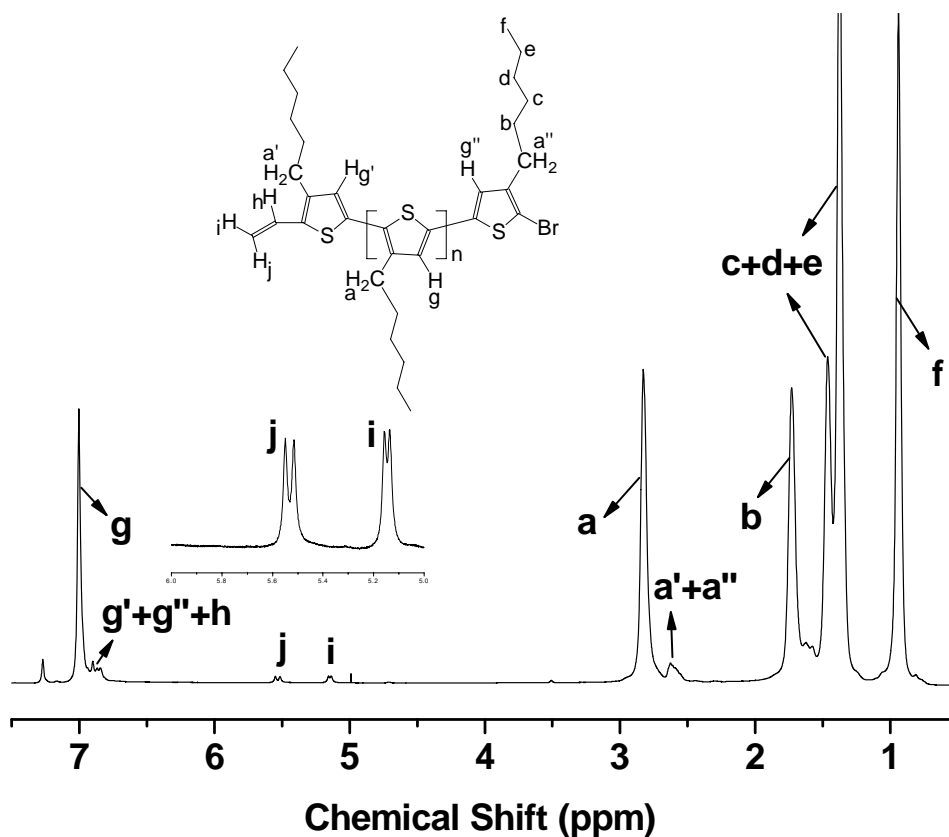


Figure 2-2. ¹H NMR spectrum of P3HT.

2.2.2 Reagents

Spectroscopic grade chloroform was purchased from Sigma-Aldrich. A.C.S. reagent grade methanol was purchased from Fisher Scientific. A.C.S. reagent grade tetrahydrofuran was also purchased from Fisher Scientific, and was dried by passing it through two columns of alumina in a Grubb's System for solvent purification.

2.2.3 Fractionation

A sample of P3HT₄₁ (2.310 g) with 41 3HT units, was dissolved in THF. The

solution was then added into methanol in order to precipitate the polymer. This precipitate was subsequently filtrated and washed with a mixture of water and methanol (1/9, v/v). The polymer was then dried with a yield of 2.156 g (yield = 93%).

The dried polymer was extracted with acetone in a Soxhlet apparatus until the extracting acetone solvent became colorless. The acetone solution was then removed by rotary evaporation to yield 0.050 g of product (yield shown in Table 2-1). To ensure purity, the acetone fraction was re-dissolved in THF and centrifuged at 2500 G to remove any remaining insoluble particle before drying to yield sample T1.

After obtaining the acetone fraction of the polymer P3HT₄₁, the remaining fractions of the polymer were then Soxhlet extracted consecutively with hexane and dichloromethane. The hexane and dichloromethane-extracted fractions are denoted as samples T2 and T3, respectively (see Table 2-1). In order to obtain higher molecular weight polymers, two P3HT samples, named T4 and T5, were each synthesized separately. T4 and T5 had average molecular weights of 8700 and 10500 g/mol, respectively.

Table 2-1. Fractionation results of P3HT₄₁.

Sample Name	Extraction Solvent	M_n^a (g/mol)	Weight (g)	Weight Fraction	Repeat Units ^b
T1	acetone	4.2×10^3	0.050	2.3%	25
T2	hexane	5.5×10^3	1.041	48.3%	33
T3	dichloromethane	7.5×10^3	1.065	49.4%	45

a: characterized by GPC, THF as solvent, $T = 25.0$ °C, flow rate = 1 mL/min.

b: the molecular weight of 3HT unit is 166 g/mol.

2.2.4 Refractive Index Increment Measurement

The refractive index increment (dn/dc) of P3HT was measured in dilute THF solution in the off-line mode with the Optilab rEX differential refractive index (DRI) detector. The experiments were conducted at a constant temperature (25.0 °C) and at a flow rate of 0.33 mL/min with a syringe pump (model R99, RAZEL) connected directly to the DRI detector.

The P3HT samples were dried in a vacuum overnight and then these dried samples were immediately weighed. Due to the drying of these samples, mass errors due to the presence of moisture were minimized. A 15.0 mg sample was fully dissolved in 6.0 mL of THF and centrifuged at 2000 G to remove any remaining dust. A stock solution of P3HT was prepared with an original concentration of 2.50×10^{-3} g/ml. Then the solution was subsequently diluted to prepare four other solutions, with descending concentrations of 2.00×10^{-3} , 1.50×10^{-3} , 1.00×10^{-3} , and 0.50×10^{-3} g/ml, respectively. Pure THF solvent was first eluted through the detector cell in order to establish a stable baseline. Once the baseline was established, each solution was passed through the DRI detector, starting with the lowest concentration. The changes in the refractive index values were recorded. This experiment was repeated three times for better accuracy, and the dn/dc value of the polymer was calculated by averaging the three data sets. The data were collected and reduced with the ASTRA version 5.3.4.10 software package provided by Wyatt Technology Corp.

2.2.5 Gel Permeation Chromatography Instrumentation

Gel permeation chromatography (GPC) analyses were carried out on a set of three μ -styragel columns (MZ Analysentechnik) with packing particles having pore diameters of 500, 10^4 , and 10^5 Å. The columns show a linear separation in the range of 5.0×10^2 to 1.0×10^6 g/mol, and they were placed in a thermostatted column compartment at 25 °C. A Wyatt Dawn Hellos-II multi-angle light scattering detector (Wyatt Technology Corp.) and a Wyatt Optilab refractive index detector were used to measure light scattering and refractive index, respectively. The laser sources of both of these detectors operated at 690 nm.

Each polymer solution was filtered through a 0.45 μ m teflon syringe filter (National Scientific) before injection. GPC analyses were performed on THF solutions at 25 °C (conc. 5 mg/mL) with their eluent rates set to 1 mL/min. The data acquisition was carried out by the ASTRA version 5.3.4.10 software package provided by Wyatt Technology Corp. The number of repeat units of the P3HT polymers (Table 2-2) were calculated according to the measured molecule weight of the P3HT polymers (as determined by GPC) divided by the molecular weight of the monomer, which is 166 g/mol.

2.2.6 Ultraviolet-Visible Spectroscopy

All P3HT solutions studied by UV-visible analysis were prepared using

spectroscopic grade chloroform. The concentrations of the solutions varied between 2.0×10^{-3} and 1.8×10^{-2} mg/mL. UV-visible measurements were carried out using a Cary 300 Bio spectrophotometer from Varian, with a spectral range from 300 to 800 nm. 10 mm Varian quartz cells were used for all measurements, and spectrograde chloroform was used as the blank.

In order to prepare P3HT thin films, a chloroform solution of P3HT was spin-coated on a pre-cleaned glass plate (Fisherbrand, Microscope Slides) at a speed of 1000 rpm for 50 seconds. These films were subsequently annealed at room temperature under high vacuum for 12 h. The dried samples were then placed in a plate holder for UV analysis.⁹ The absorbance was kept below 1.0 for both solution and thin film UV-visible analysis, in order to minimize measurement errors.

2.2.7 Fluorescence Measurements

P3HT solutions were prepared at a concentration of 2.0×10^{-3} mg/mL in chloroform. Fluorescence measurements were performed with a Photon Technology International Alphascan spectrophotometer with a 150 W xenon compact light source, using 10 mm Hellma quartz cells. The absorbance of the solutions was kept at 0.1. The excitation wavelength was 430 nm, and the excitation and emission slit widths were set at 5 and 3 nm, respectively. The fluorescence spectra of the P3HT thin films were obtained from the spin-coated films used in the UV-visible experiments.

2.3 Experimental Results

2.3.1 Molecular Weight

A series of five samples were prepared and named from lowest to highest molecular weight, as samples T1, T2, T3, T4, and T5. Each sample varied in molecular weight by more than 1000 g/mol and was obtained by the method described in Section 2.2.1. The regioregularities were all above 90%. According to the GPC curves (Figure 2-3), the five samples have a molecular weight range between 4200 and 11000 g/mol, and their polydispersities were no higher than 1.20, which is lower than previous reports.^{2,4-7} A complete summary of the molecular characterization is given in Table 2-2.

Table 2-2. Summary of the five P3HT samples.

Sample Name	M_n (g/mol)	M_w (g/mol)	Repeat Units (GPC method)	PDI	Repeat Units (NMR method)	RR ^a
T1	4200	5000	25	1.20	27	91%
T2	5500	6100	33	1.10	34	92%
T3	7500	8900	45	1.19	46	92%
T4	8700	9600	53	1.12	55	94%
T5	10500	11900	63	1.13	67	95%

a: RR denotes for regioregularity

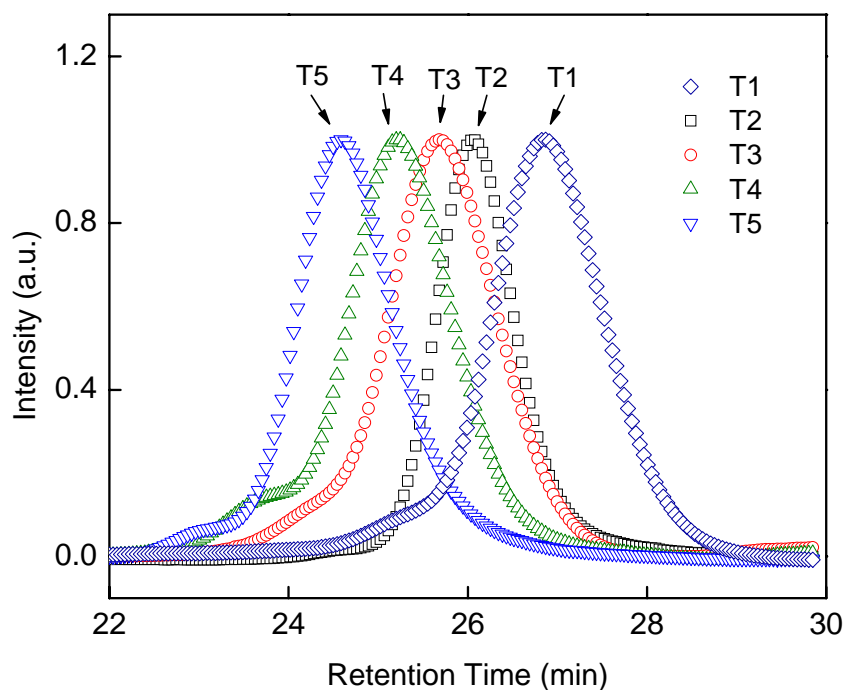


Figure 2-3. GPC plot of the five P3HT samples: T1, T2, T3, T4, T5.

2.3.2 Refractive Index Increment

The refractive index increment (dn/dc), an important parameter for GPC analysis, was measured first. From the change in the differential refractive index increment (DRI) detector voltage (ΔV), the difference in the refractive index between that of a pure solvent and the polymer solution (Δn) for each concentration can be calculated from $\Delta n = \alpha \Delta V$ (where α is the DRI calibration constant). Figure 2-4 represents a typical plot of sample T3 with Δn as a function of the polymer concentration c . The slope in this plot equals $d(\Delta n)/dc$, or dn/dc , a unique property of that polymer in that particular solvent at that temperature and wavelength. The value of dn/dc obtained for T3 was 0.277 mL/g. For

all dn/dc measurements, the straight line passed through the origin, indicating good accuracy was obtained in the experiment. Five dn/dc values are listed in the Table 2-3.

Table 2-3. Refractive index increment of P3HT samples.

Sample Name	dn/dc^a (mL/g)	M_n (g/mol)
T1	0.244	4200
T2	0.262	5500
T3	0.277	7500
T4	0.280	8700
T5	0.283	10500

a: THF as solvent, $T = 25.0$ °C, flow rate = 0.33 mL/min, Laser $\lambda = 638$ nm.

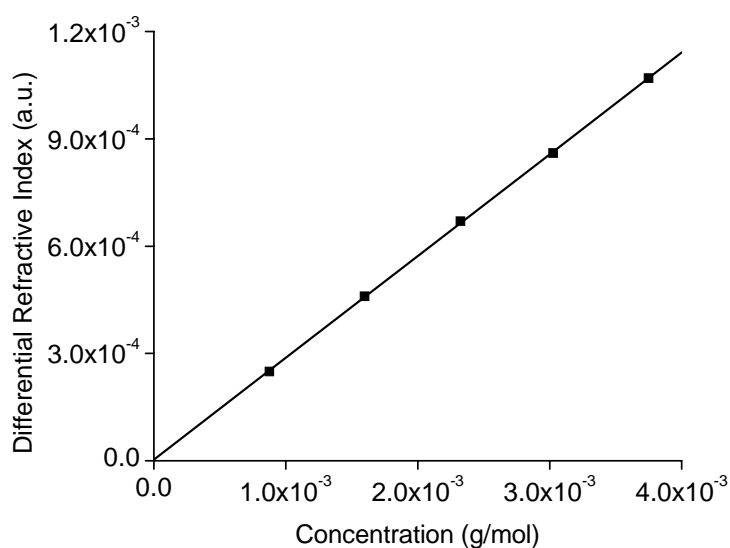


Figure 2-4. A typical plot of differential refractive index versus the concentration of sample T3 in the THF solution.

2.3.3 UV-visible Spectra

The UV-visible spectra of the P3HT samples were measured while dissolved in chloroform solution and as thin films. The maximum absorption wavelengths (λ_{\max}), extinction coefficients (ϵ), and emission wavelengths of both states (λ_{em}), in solution and

as thin films, are listed in Table 2-4. The spectra of the five samples in chloroform solution and as a spin-coated thin film of P3HT are shown in Figures 2-5 and 2-6, respectively. For example, T3 exhibits a λ_{max} at 450 nm when dissolved in chloroform and at 541 nm as a thin film. This indicates that the packing of the polymer chains in the condensed phase should favor a coplanar arrangement of the adjacent thiophene rings. This results in a red shift in the λ_{max} when compared with the solution-phase polymer.

Table 2-4. UV-visible spectral properties of P3HT samples.

Sample Name	$\lambda_{\text{max}} / \text{nm}$ (solution)	ϵ ($\text{L mol}^{-1} \text{ cm}^{-1}$)	$\lambda_{\text{max}} / \text{nm}$ (thin film)	M_n (g/mol)
T1	439	4700	478	4200
T2	448	7500	537	5500
T3	450	7800	541	7500
T4	451	7900	549	8700
T5	451	8000	550	10500

The thin films of the P3HT samples were prepared by spin-coating from the chloroform solutions of the polymer. The absorption spectrum features vibrational fine structures, such as two shoulder peaks on both sides of the maximum absorption peak, which were enhanced by coplanarization and the corresponding π -electron delocalization. However, due to the immobility of the conjugated polythiophene chains, the peaks were not very smooth. For example, Sample T3 displayed a red-shifted maximum absorption peak at 541 nm, which had shoulders at 525 and 597 nm. These correspond to energy levels of 2.27 eV (541 nm), 2.39 eV (525 nm), and 2.08 eV (597 nm), respectively. The energy differences between the peak and each of the shoulders, and between the two

shoulders are roughly 0.19 and 0.12 eV. This may also correspond with electronic transition between different vibration energy levels in the conjugated polymer backbone.¹¹

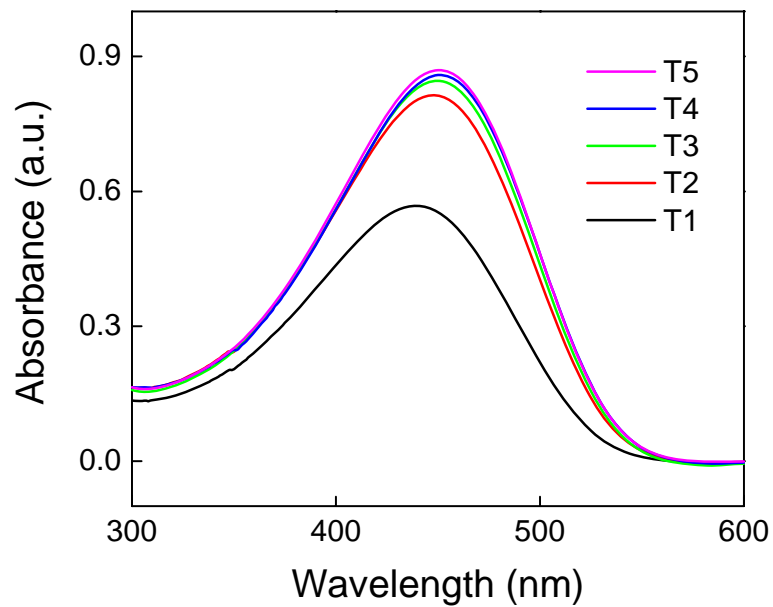


Figure 2-5. UV-visible absorption spectra of P3HT samples in chloroform solutions.

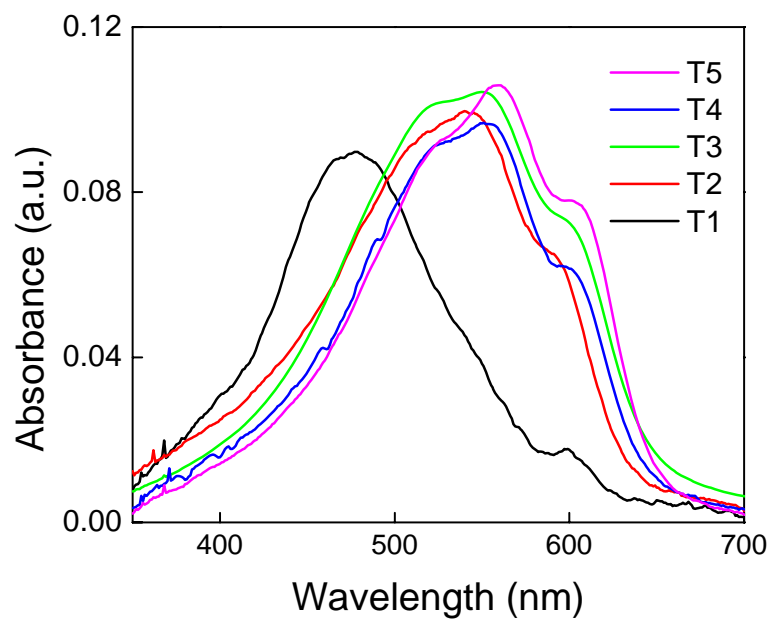


Figure 2-6. UV-visible absorption spectra of P3HT samples as thin films.

2.3.4 Fluorescence Spectra

Fluorescence measurements of dilute polymer solutions of P3HT were also recorded. All details have been listed in Table 2-5 and typical fluorescence spectra in solution and as a thin film for T3 are shown in Figure 2-7 and Figure 2-8, respectively. As shown in Table 2-5, maxim emission wavelength of the solution state red-shifted from 570.5, to 573.5, to 575, and to the final value of 575.5 nm, as one progressed from the T1 sample through to the T5 sample. A similar trend was observed with the thin film samples of this polymer, with wavelength changing from 643.5, to 649, to 653, to 655 nm, and to 656 nm, as one progressed from the T1 sample through to the T5 sample. However, the shifts in the emission wavelength in solution from T1 to T5 are less than those found for the polymers in the thin film state. In a similar manner to the analysis provided in the UV-visible study, this can be explained by the ordering of the P3HT chains and their packing after spin-coating when compared with the twisted chain conformation in chloroform solutions. Due to self-quenching in a thin film, the fluorescence spectra were much weaker than those found in solution, and the Stokes shift for T1 through T5 increases with the molecular weight.

Table 2-5. Fluorescence properties of P3HT samples.

Sample Name	λ_{em}/nm (chloroform solution)	λ_{em}/nm (thin film)	M_n (g/mol)
T1	570.5	643.5	4200
T2	573.5	649.0	5500
T3	575.0	653.0	7500
T4	575.5	655.0	8700
T5	575.5	656.0	10500

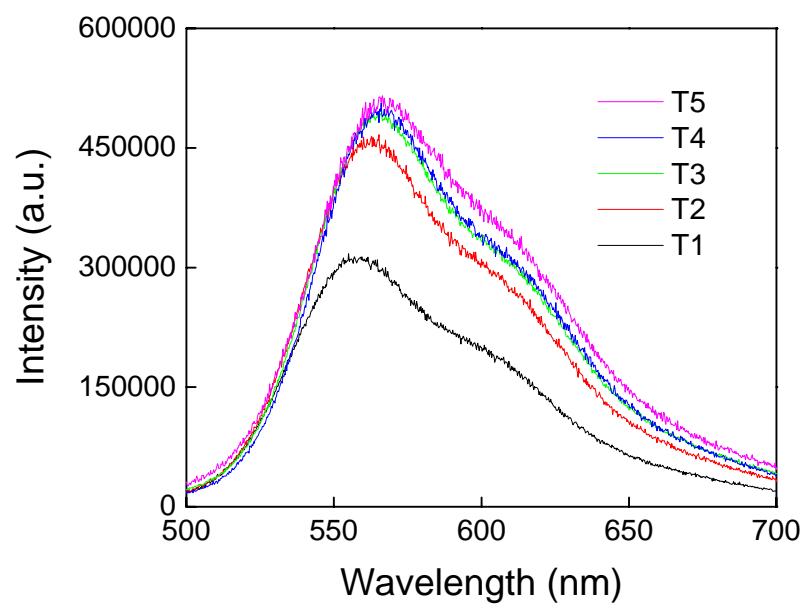


Figure 2-7. Fluorescence spectra of P3HT samples in chloroform solutions.

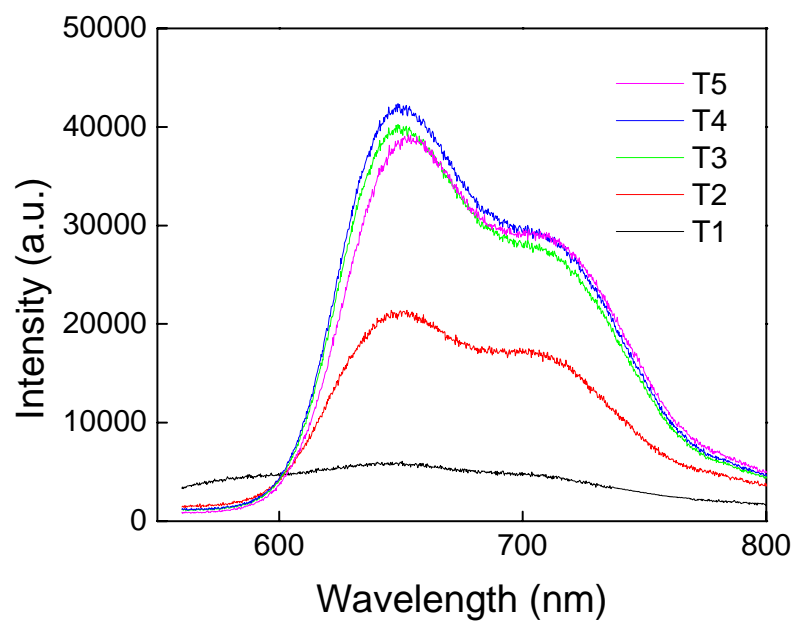


Figure 2-8. Fluorescence spectra of P3HT samples as thin films.

2.4 Discussion of the Properties Affected by the Molecular Weight of P3HT

2.4.1 Refractive Index Increment

The dn/dc values increased from 0.24 to 0.28 mL/g with increasing molecular weight (Figure 2-9). These results are consistent with the accepted pattern dn/dc increase for polymers with low molecular weights and levels off for polymers with higher molecular, e.g. >10,000 g/mol. By combining the results from the study of the five different P3HT samples, we determined:

$$dn/dc \text{ (mL/g)} = 0.316 - 298/M_n \text{ (g/mol)}$$

The dn/dc value of 0.307 mL/g reported in the literature¹⁰ for P3HT with a molecular weight of 223,000 g/mol agrees closely with this equation, indicating a potential method for the determination of the molecular weight, and hence, certain physical properties, of P3HT from its dn/dc values. In addition, other polymers such as poly(ethylene oxide) (PEO), poly(methyl methacrylate) (PMMA), and polystyrene (PS), have dn/dc values ranging from 0.11 to 0.20 mL/g.¹¹⁻¹³ The high dn/dc value of P3HT can be attributed to the existence of the sulfur atoms in the thiophene units, which contribute to give a large refraction index.¹⁴

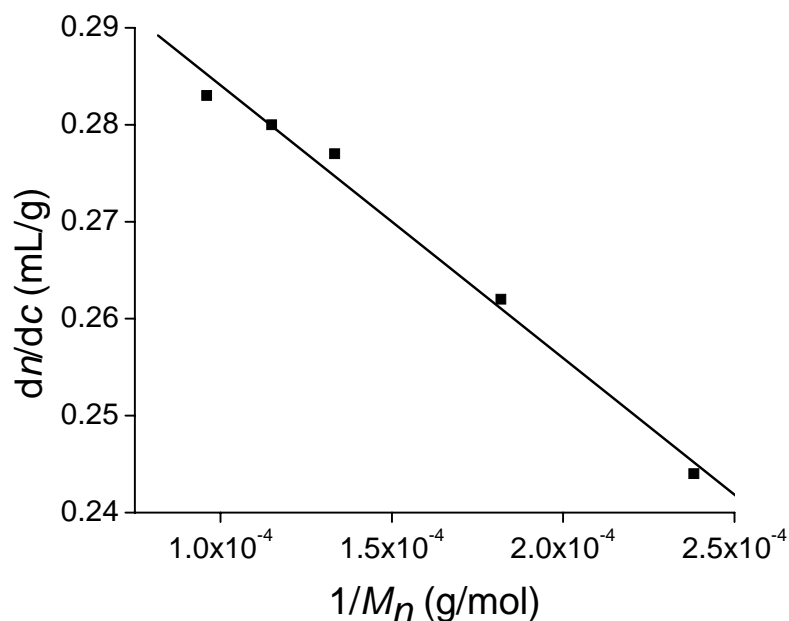


Figure 2-9. Schematic representation of the relationship between the refractive index increment of each P3HT sample in THF solution and its molecular weight.

2.4.2 Spectral Properties

When dissolved in solution or as a thin film, the absorption and emission peaks of the samples exhibit red shifts as their molecular weight increases. This is considered to originate from the decrease of the π - π^* transition energy of P3HT. Figures 2-10 and 2-11 help to summarize the relationship between the absorption and emission wavelengths (determined from UV-visible and fluorescence spectroscopies, respectively) and the molecular weight. An increase of molecular weight among the P3HT samples corresponds with the presence of additional units in the polymer backbone, which can facilitate the formation of coplanar P3HT chains and result in longer effective conjugation lengths. Therefore, the π -electrons in a longer P3HT chain will be

subjected to a greater amount of delocalization and thus decrease the π - π^* transition band-gap, resulting in the red shift observed in the spectra.

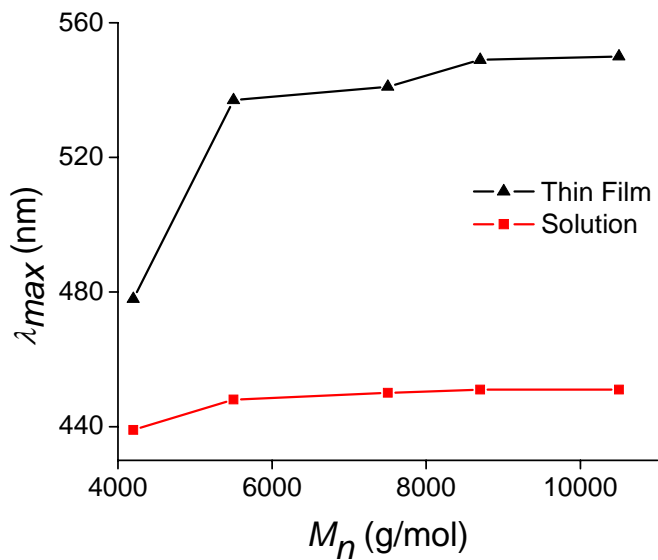


Figure 2-10. Schematic representation of the relationship between λ_{max} and molecular weight of P3HT in chloroform solution and as a thin film.

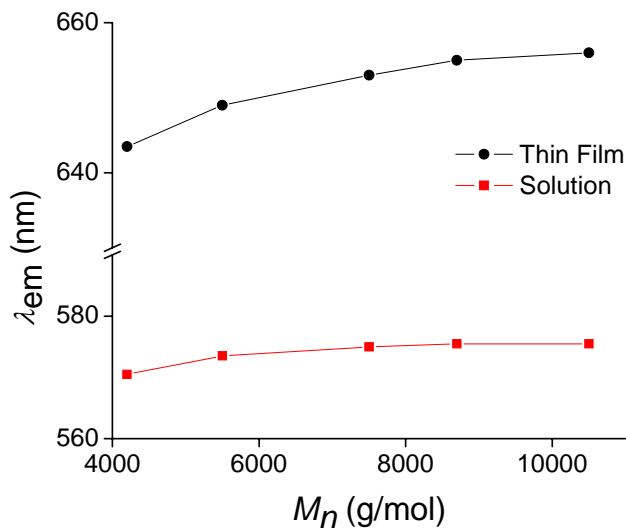


Figure 2-11. Schematic representation of the relationship between λ_{em} and the molecular weight for P3HT samples in chloroform solution and as a thin film.

2.4.3 Extinction Coefficient

In addition, it was found that a correlation also exists between the molecular weight and the extinction coefficient for T1 through T5. For each sample, solutions were prepared in chloroform with varying concentrations. The absorbance at the maximum wavelength of each sample was measured and plotted against concentration to obtain the extinction coefficient, ϵ . The values of the extinction coefficient were plotted against the molecular weight, as shown in Figure 2-12. The value of ϵ at the maximum absorption increases from 4700 to 8000 L mol⁻¹ cm⁻¹ with increasing molecular weight. It can be inferred from Figure 2-12 that only a slight increase of ϵ will occur in the region above 1×10^4 g/mol. This trend could explain the previously reported value of 8800 L mol⁻¹ cm⁻¹ for a P3HT sample having a high molecular weight of 4.8×10^4 g/mol.¹⁵ The slight change of the extinction coefficient, ϵ , with different molecular weights may originate from the difference in the solvent-polymer interaction, which corresponds to the different lengths of the polymer in the solvent, chloroform.

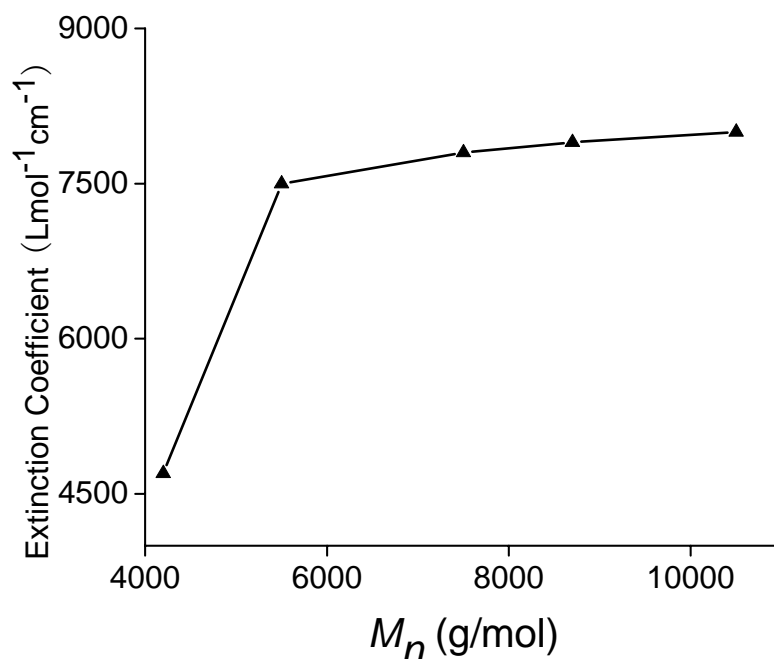


Figure 2-12. Schematic representation of the relationship between the extinction coefficient of each P3HT sample in chloroform solution and its molecular weight.

2.4.4 Conjugation Length

An important motivation for studying conjugated polymers with varying molecular weights is to establish a relationship between the effective conjugation length and its effect on the regulation of the characteristics of the incorporated polythiophenes. Compared with the previous studies, the P3HTs studied here, which have regioregularities higher than 90% and polydispersities less than 1.25, can offer more convincing results because of their well-defined structure. P3HTs with relatively low molecular weights ($< 200,000$ g/mol) showed strong π - π^* electron absorption bands in the visible region,¹⁰ which were red-shifted with increasing chain length.

Previous studies have attempted to determine effective conjugation length of P3HT. Hoeve *et al.* concluded that the effective conjugation of the polythiophene is not longer than 11 repeat units.¹⁶ However, a later study based on the extrapolation of the transition energy and chain length relationship suggested that the saturation of the effective conjugation may be extended to no more than 20 thiophene units.¹⁷ Our study of regioregular P3HT polymers shows that the absorption spectra shifted to 450 nm in solution and to 541 nm in thin films, which was initially observed for the T3 sample, which had 45 repeat units. The λ_{\max} values of our series of P3HT polymers increased significantly as their number of repeat units was increased, from 25, to 35, and up to 45 repeat units. Beyond this point, as the number of repeat units was increased up to 53 and 63 repeat units, only negligible increases of the λ_{\max} values were observed. From this, we can conclude that conjugation length of the P3HT polymer described in this study is at least 45 units. It is worth noting that the two absorption bands of the highest molecular weight sample described in this study, T5, are longer than those found in previous reports describing P3HT,¹⁸ which were observed at 443 nm in solution and 526 nm in solid thin films. Thus, it can be inferred that the reason why the effective conjugation length of P3HT has been extended up to 45 repeat thiophene units in this study, is probably due to the very high regioregularities and low polydispersities of these samples. Compared with the study of a series of well-defined poly(3-octylthiophene) derivatives,¹⁹ where a continuous red shift in their absorption spectra for polymers up to 72 repeat units was observed, it is believed that the higher-ordered P3HT structure can

offer a longer effective conjugation length.

2.5 Conclusions

From the five P3HT samples, the relationship between the molecular weight and the refractive index increment was obtained. Also, the relationship between molecular weight and spectral information, such as, the molar absorptivity, and the fluorescence spectra was determined. The data shows that the refractive index increment (dn/dc), maximum absorption wavelength, extinction coefficient, and maximum emission wavelength all increase with increasing the molecular weight for the relatively low molecular weight P3HT studied here ($< 200,000$ g/mol), which indicates a possible relationship among these factors. Revealing the correlation between the molecular weight and the optical and spectral properties of P3HT (below 1.5×10^4 g/mol) can offer a reference for the later study of P3HT-containing diblock copolymers. These results may serve as benchmarks for subsequent studies of the use of polythiophene-based materials towards applications as biosensors, and also for the comparison of the physical properties of polythiophene derivatives. These developments can serve as useful models for tailoring the properties of P3HT to meet specific applications.

References

- 1 Kline, R. J.; McGehee, M. D.; Kdnikova, E. N.; Liu, J.; Frechet, J. M. J. *Adv. Mater.* **2003**, *15*, 1519.
- 2 Brinkmann, M.; Rannou, P. *Macromolecules* **2009**, *42*, 1125-1130.
- 3 Sirringhaus, H.; Brown, P. J.; Friend, R.H.; Nielsen, M. M.; Bechgaard, K.; Langeveld-Voss, B. M. W.; Spiering, A. J. H.; Janssen, R. A. J.; Meijer, E. W.; Herwig, P.; De Leeuw, D. M. *Nature (London)* **1999**, *401*, 685.
- 4 Verilhac, J.-M.; LeBlevenec, G.; Djurado, D.; Rieutord, F.; Chouiki M.; Travers, J.-P. Pron, A. *Synthetic Metals* **2006**, *156*, 815-823.
- 5 Xu, B.; Holdcroft, S. *Macromolecules* **1993**, *26*, 4457-4460.
- 6 Heffner, G. W.; Pearson D. S. *Macromolecules* **1991**, *24*, 6295-6299.
- 7 Xu, B.; Lowe, J.; Holdcroft, S.; *Thin Solid Films*, **1994**, *243*, 638-642.
- 8 Jeffries-El, M.; Sauv e, G.; McCullough, R. D. *Macromolecules* **2005**, *38*, 10346-10352.
- 9 Li, G.; Yao, Y.; Yang, H.; Shrotriya, V.; Yang, G.; Yang, Y. *Adv. Funct. Mater.* **2007**, *17*, 1636-1644.
- 10 Heffner, G. W.; Pearson D. S. *Macromolecules* **1991**, *24*, 6295-6299.
- 11 Fragouli, P. G.; Iatrou, H.; Hadjichristidis, N. *Polymer* **2002**, *43*, 7141-7144.
- 12 Tumoloa, T.; Angnes, L.; Baptista M. S. *Analytical Biochemistry* **2003**, *333* 273-279.
- 13 Sauzedde, F.; Hunkeler, D. *J. Polym. Anal. Charact.* **2001**, *6*, 295-314.
- 14 You, N.-H.; Suzuki, Y.; Yorifuji, D.; Ando, S.; Ueda, M. *Macromolecules* **2008**, *41*, 6361-6366.
- 15 Linton, J. R.; Frank, C. W.; Rughooputh, S. D. D. V. *Synth. Met.* **1989**, *28*, C393-C398.
- 16 Havinga, E. E.; Rotte, I.; Meijer, E. W.; ten Hoeve, W.; Wynberg, H. *Synth. Met.* **1991**, *41*, 473-478.
- 17 Meier, H.; Stalmach, U.; Kolshorn, H. *Acta Polymer.* **1997**, *48*, 379-384.
- 18 McCullough, R. D.; Lowe, R. D.; Jayaraman, M.; Anderson, D. L. *J. Org. Chem.* **1993**, *58*, 904-912.
- 19 Izumi, T.; Kobashi, S.; Takimiya, K.; Aso, Y.; Otsubo T. *J. Am. Chem. Soc.* **2003**, *125*, 5286-5287

Chapter 3. Morphological and Spectral Properties of Poly(3-hexyl thiophene)-*block*-Poly(2-hydroxyethyl methacrylate) in Various Solvents

3.1 Introduction

The aggregation of rod-coil block copolymers in solution have yielded a number of micellar morphologies, such as lamellae, spheres, cylinders, and vesicles structures.^{1,2} These morphologies are driven not only by the solvent selectivity, but are also influenced by the volume fraction of the rigid rod block. The combination of coil blocks with the rigid poly(3-hexyl thiophene) (P3HT) block can result in the formation of self-assembled morphologies, such as spheres,³ fibrils,⁴ lamellae,⁵ or nanowires.⁶ At the same time, it can change the electronic^{4,7} and optoelectronic^{8,9} properties of the copolymer from those of the pristine P3HT homopolymer.

Recently, most studies of P3HT block copolymers have focused on the bulk solid state, which is prepared as thin film, because of their potential application in solar cells.^{4,7} To the best of our knowledge, the potential morphological changes of P3HT rod-coil block copolymer micelles induced by coil length and solvent quality, have not yet been explored. Therefore in this study, the morphology and spectral properties of poly(3-hexyl thiophene)-*block*-poly(2-hydroxyethyl methacrylate) (P3HT-*b*-PHEMA) with different block lengths were investigated, to understand the mechanism of the

self-assembly of micelles.

3.2 Materials and Methods

3.2.1 Polymer Synthesis and Characterization

Three poly(3-hexyl thiophene)-*block*-poly(2-hydroxyethyl methacrylate), (P3HT-*b*-PHEMA) diblock copolymers, with different numbers of repeat units, including P3HT₃₀-*b*-PHEMA₈₀, P3HT₄₁-*b*-PHEMA₈₂, and P3HT₅₃-*b*-PHEMA₆₀, were prepared by Dehui Han for this study. These polymers were obtained from their precursors, poly(3-hexyl thiophene)-*block*-poly(2-trimethylsiloxyethyl methacrylate), (P3HT-*b*-P(HEMA-TMS)), and the P(HEMA-TMS) block was made by living anionic polymerization. The trimethylsiloxane protecting groups were subsequently removed by hydrolysis in THF/MeOH (volume fraction $v/v = 1/2$), as shown in Figure 3-1.

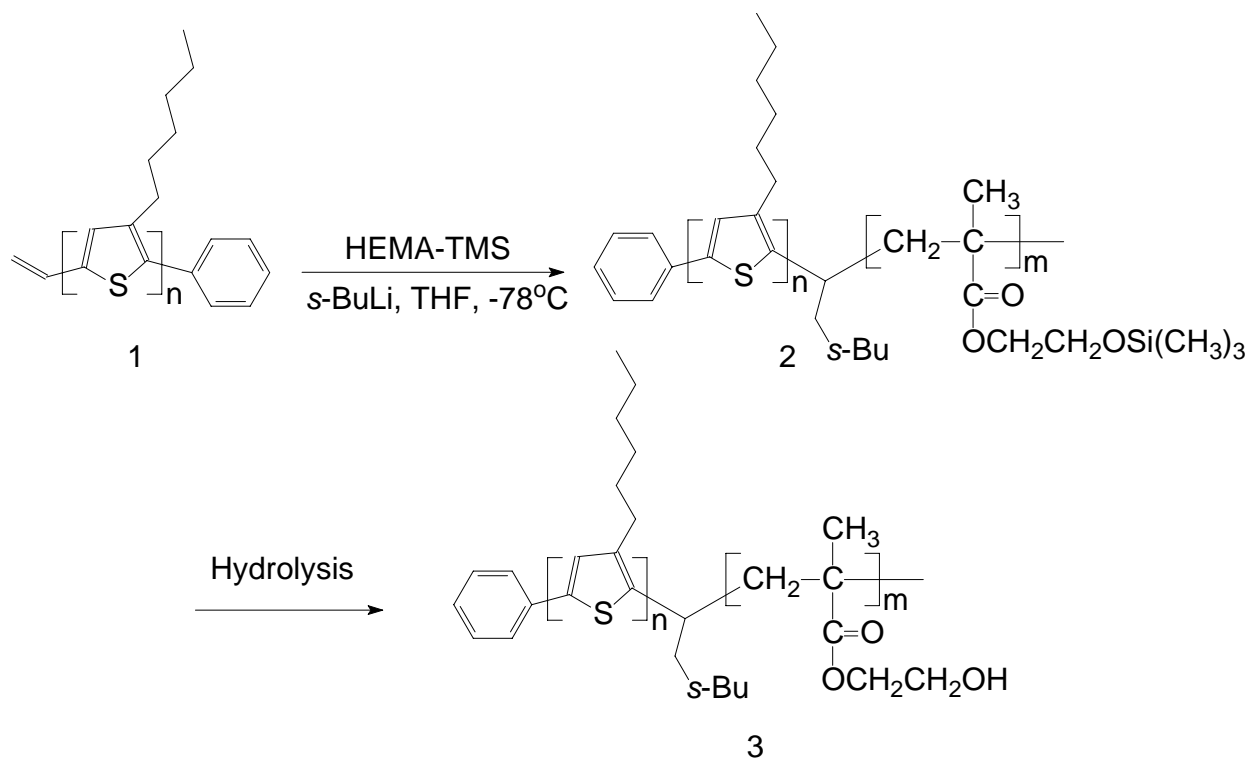


Figure 3-1. Schematic representation of synthesis of P3HT-*b*-PHEMA.

In order to synthesize P3HT₅₃-*b*-P(HEMA-TMS)₆₀, for example, P3HT (**1**, $M_n = 8700$ g/mol, 0.60 g) and LiCl (18.0 mg) were added into a polymerization flask, and dried under vacuum overnight. Freshly distilled THF (400 mL) was added in one addition into the flask to dissolve the P3HT macroinitiator (**1**). This solution was then cooled to -78°C , and excess *sec*-butyl lithium in hexane (1.4 M, 0.35 mmol, 0.25 mL) was then added slowly into the polymerization system *via* syringe. After one hour, the *sec*-butyl lithium was deactivated by warming the solution to 40°C , for 20 min. The macroinitiator solution was again cooled to -78°C , and monomer HEMA-TMS (0.90 mL) was then added drop-wise into the reaction flask by syringe. After stirring for one hour, degassed methanol (2.0 mL) was added in order to quench the polymerization. In order

to hydrolyze the P(HEMA-TMS) block (**2**) to PHEMA, methanol (100 mL) and water (5 mL) were added into the polymerization flask, and the mixture stirred overnight. The crude diblock copolymer P3HT₅₃-*b*-PHEMA₆₀ (**3**) was purified by extracting it with toluene at room temperature. In order to calculate the molecular weights, we transformed P3HT-*b*-PHEMA into poly(3-hexyl thiophene)-*block*-poly(2-cinnamoyloxy ethyl methacrylate (P3HT-*b*-PCEMA) with cinnamoyl chloride. This reaction improved the solubility of PHEMA blocks in THF and chloroform. For convenience, P3HT₃₀-*b*-PHEMA₈₀, P3HT₄₁-*b*-PHEMA₈₂, and P3HT₅₃-*b*-PHEMA₆₀ were abbreviated as DC1, DC2, and DC3, respectively. Three diblock copolymers were subsequently characterized by ¹H NMR and GPC analyses, in order to determine the repeat unit numbers of P3HT and PHEMA,, and polydispersity of diblock copolymer, respectively. A summary is given in Table 3-1.

Table 3-1. Summary of the diblock copolymers of P3HT-*b*-PHEMA.

Sample Name	3HT Units	HEMA Units	M_n (g/mol)	M_w (g/mol)	PDI
DC1	30	80	27200	30500	1.12
DC2	41	82	23200	27600	1.19
DC3	53	60	29600	34600	1.17

3.2.2 Micelle Preparation

Sample solutions were prepared by first dissolving the copolymers into a solvent mixture that could dissolve both blocks, such as a THF/MeOH mixture (v/v = 94/6), with an initial polymer concentration of 0.75 mg/mL. These solutions were then equilibrated by stirring overnight. The solutions used in this study were prepared by adding

methanol, a selective solvent for the PHEMA block, drop-wise into the block copolymer solution under moderate magnetic stirring. Various copolymer solutions, with different THF/MeOH volume fractions, including 70/30, 55/45, 40/60, and 20/80 were prepared. Another micellar solution, with a THF/MeOH volume fraction of 1/99, was prepared by directly adding the THF/MeOH solvent mixture to the copolymer. The polymer concentrations were kept at 0.15 mg/mL. In order to prepare a micellar solution with a final composition of THF/MeOH, v/v = 70/30, P3HT-*b*-PHEMA (0.75 mg) was first fully dissolved in 1.00 mL of a THF/MeOH (v/v = 94/6) solvent mixture. Methanol (0.34 mL) was then added drop-wise under vigorous stirring, to increase the methanol volume fraction to 30%. Stirring was continued for 12 hours, after which the solution was diluted to a final volume of 5.00 mL (final concentration 0.15 mg/mL) with the addition of a 3.66 mL portion of the THF/MeOH solvent mixture (v/v = 70/30). The solution was then stirred for 24 hours prior to characterization, in order to reach the equilibrium morphologies.

3.2.3 Transmission Electron Microscopy

Micellar solutions with concentrations of 0.15 mg/mL, were sprayed onto nitrocellulose coated copper grids, with the aid of a home-made atomizer. The samples were stained with a 2 wt% phosphotungstic acid solution, to stain the background and highlight the entire assemblies. TEM images were recorded on a Hitachi H-7000 transmission electron microscope with an accelerating voltage of 75.0 kV, and

magnifications between 80,000x and 150,000x. All of the specimens were dried under vacuum before characterization. Electron diffraction patterns were obtained directly on dried micelles.

3.2.4 Atomic Force Microscopy

The sample solutions were sprayed with the aid of an aspirator onto freshly cleaved mica surfaces. The specimens were then imaged immediately after drying. AFM imaging was performed on a Veeco quadrexed Multimode III, with a J vertical scanner. All images were taken in air using tapping mode, with silicon probes (Veeco-RTESP). The scan frequency was kept at 1.0 Hz, while the scan size ranged from 0.5 to 5 μm . During acquisition, topographical and phase images were recorded at the same time.

3.2.5 Dynamic Light Scattering

Light scattering measurements were carried out on a Brookhaven BI-200SM Goniometer, with a BI-9000AT digital correlator, and a He-Ne laser ($\lambda = 632.8 \text{ nm}$) at a measurement angle of 90° . The autocorrelation function, hydrodynamic diameter and the polydispersities were calculated automatically by the software supplied (BI-ZP Version 4.0, Brookhaven Instrument Corporation). Light scattering cells and micropipette tips were rinsed three times with a THF/MeOH mixture (v/v = 1/99) that was clarified by a 0.1-micron PTFE filter. Sample solutions were filtered twice through a 0.45 micron PTFE filter. The solutions were transferred into clean light scattering

cells, and the cells were immediately capped and double-sealed with PTFE tape. DLS measurements were recorded immediately. The viscosity and the index of refraction were calculated from the volume-weighted average of the components. Measurements were repeated ten times and the reported values are the arithmetic mean, and the error reported is the 95% confidence interval.

3.2.6 Ultraviolet-Visible Spectroscopy

All micellar solutions used for UV-visible analysis were prepared at a concentration of 5.0×10^{-2} mg/mL in a THF/MeOH mixture. UV-visible measurements were conducted on a Cary 300 Bio spectrophotometer from Varian, with a spectral range of 300 to 800 nm. Varian 10 mm quartz cells were used for all measurements, and the same THF/MeOH volume fraction mixture that was used to prepare the micellar solution was used as the blank.

3.2.7 Fluorescence Spectroscopy

Micellar solutions were prepared at a concentration of 5.0×10^{-3} mg/mL in THF/MeOH mixtures. Fluorescence measurements were performed on a Photon Technology International Alphascan spectrophotometer, with a 150 W Xenon compact light source, using 10 mm Hellma quartz cells. The absorbance of the solutions was kept at 0.10. The excitation wavelength used was 430 nm, and the excitation and emission slit widths were set at 5 and 3 nm, respectively.

3.3 Experimental Results

3.3.1 Comparison of the Micellar Properties Determined by TEM, AFM, and DLS Measurements

The micellar morphologies of the diblock copolymers were subsequently analyzed by TEM, AFM, and DLS techniques. Each sample was first prepared in THF/MeOH solvent mixtures with the following volume fractions: 70/30, 55/45, 40/60, 20/80, and 1/99 (THF/MeOH). The last batch of each sample, with a THF/MeOH volume fraction of 1/99, was analyzed by the above experiments. TEM and AFM images were used to view the morphologies of the micelles of the diblock copolymers, as well as their diameters. These results were compared with those obtained from DLS measurements. A summary of the diameters of the micelles obtained using TEM, AFM, and DLS methods is shown in Table 3-2.

Table 3-2. Diameters of the micelles of P3HT-*b*-PHEMA diblock copolymers as determined by TEM, AFM, and DLS techniques.^a

Sample Name	d_{TEM} (nm)	d_{AFM} (nm)	D_h (nm) ^b	Polydispersity of DLS K_2^2/K_4
DC1	10.1 ± 2.5	21.8 ± 6.7	33.0 ± 0.8	0.12
DC2	14.9 ± 4.2	29.1 ± 9.3	37.6 ± 0.5	0.09
DC3	18.7 ± 5.6	34.5 ± 6.1	40.4 ± 1.2	0.10

a: Values are given as the average \pm standard deviation.

b: D_h denotes for hydrodynamic diameter measured by DLS experiments. d_{TEM} and d_{AFM} denote the diameter sizes obtained from TEM and AFM, respectively.

Since electron beams that were accelerated under high voltage can penetrate through polymers, the micellar morphologies could be imaged by TEM. The P3HT block is not soluble in aqueous solution, and therefore the micellar cores will not be stained by the aqueous phosphotungstic acid staining agent, while the background will be stained. The tungsten atoms of the phosphotungstic acid are very electron-dense, so they can scatter the electrons from their path. As a result, the darker areas in the TEM images correspond to the stained background, while the lighter areas correspond to the micellar cores. Figures 3-2, 3-3, and 3-4 show TEM images of the three P3HT-*b*-PHEMA diblock copolymers, where spherical micellar morphologies were observed. The diameters of the micellar cores of DC1, DC2, and DC3 were 10.1 ± 2.5 nm, 14.9 ± 4.2 nm, and 18.7 ± 5.6 nm, respectively.

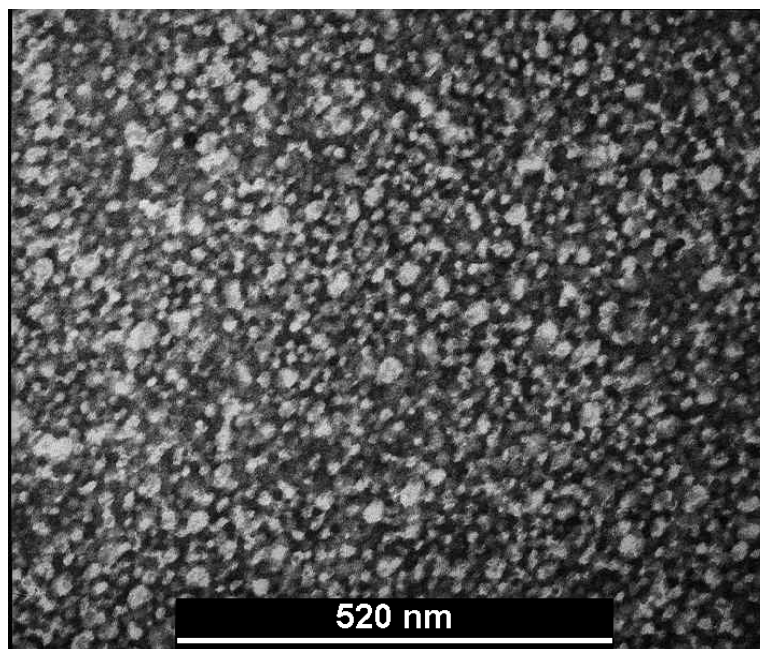


Figure 3-2. TEM image of the sample DC1 sprayed from a THF/MeOH mixture (v/v = 1/99). The sample was stained by phosphotungstic acid.

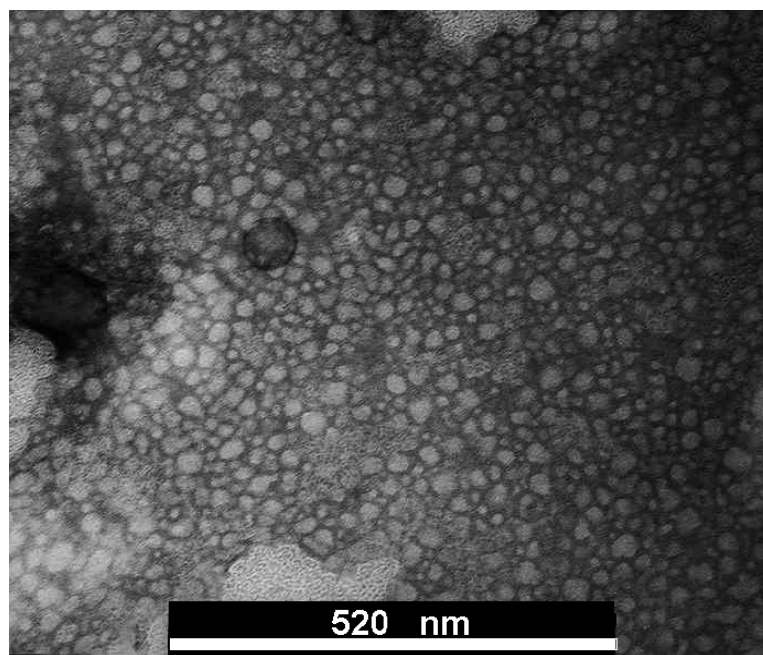


Figure 3-3. TEM image of the sample DC2 sprayed from a THF/MeOH mixture (v/v = 1/99). The sample was stained by phosphotungstic acid.

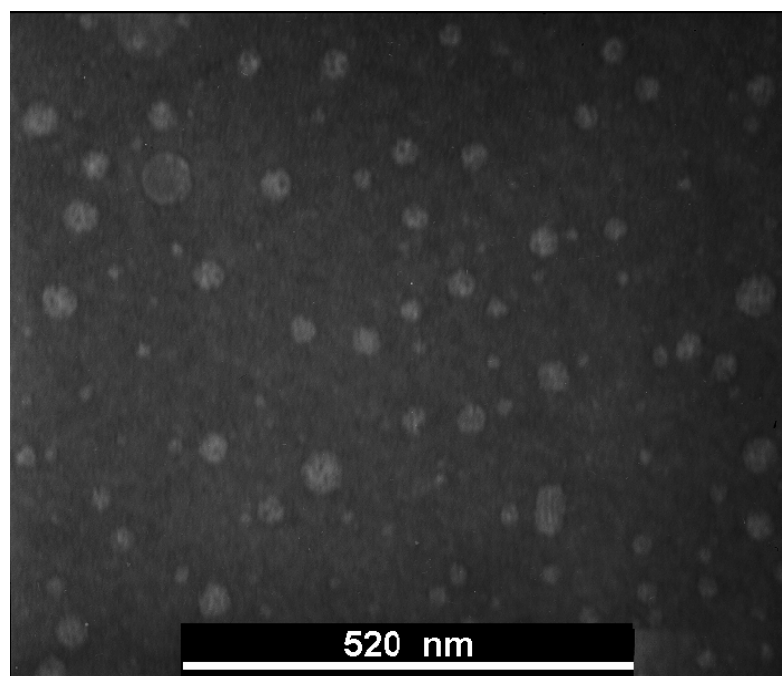


Figure 3-4. TEM image of the sample DC3 sprayed from a THF/MeOH mixture (v/v = 1/99). The sample was stained by phosphotungstic acid.

AFM images were also used to analyze the topography of the three polymer micelles. Similar to the images shown in TEM, a large number of spherical micelles were observed in the AFM images (Figures 3-5 to 3-7), and the contrast in height images (left) and phase images (right) implied that the micelles of P3HT-*b*-PHEMA had well-defined structures. With a THF/MeOH solvent mixture of volume fraction of 1/99, the average diameters of the micelles are 21.8 ± 6.7 nm for DC1, 29.1 ± 9.3 nm for DC2, and 34.5 ± 6.1 nm for DC3. These values are larger than those obtained from TEM measurements, probably because of the deformation of the micelles by the AFM tip. Based on the results above, it can be concluded that when a coil block selective solvent is used, the tendency of the block copolymer to self-assemble is enhanced, due to the phase separation and aggregation of the rigid block segments. Moreover, the information revealed by the AFM images indicates that these micellar structures have good stability, not only when they are sprayed on the carbon film of a copper grid for TEM analysis, but also on the mica surfaces used for AFM analysis.

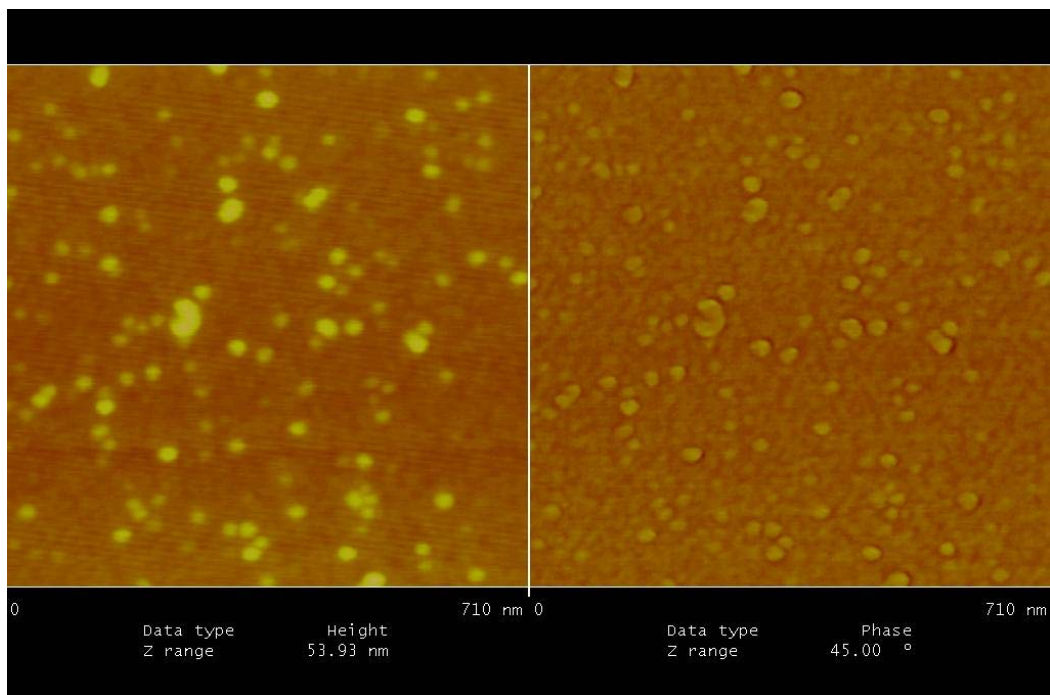


Figure 3-5. AFM topography (left) and phase (right) images of P3HT₃₀-*b*-PHEMA₈₀ sprayed from a THF/MeOH mixture (v/v = 1/99).

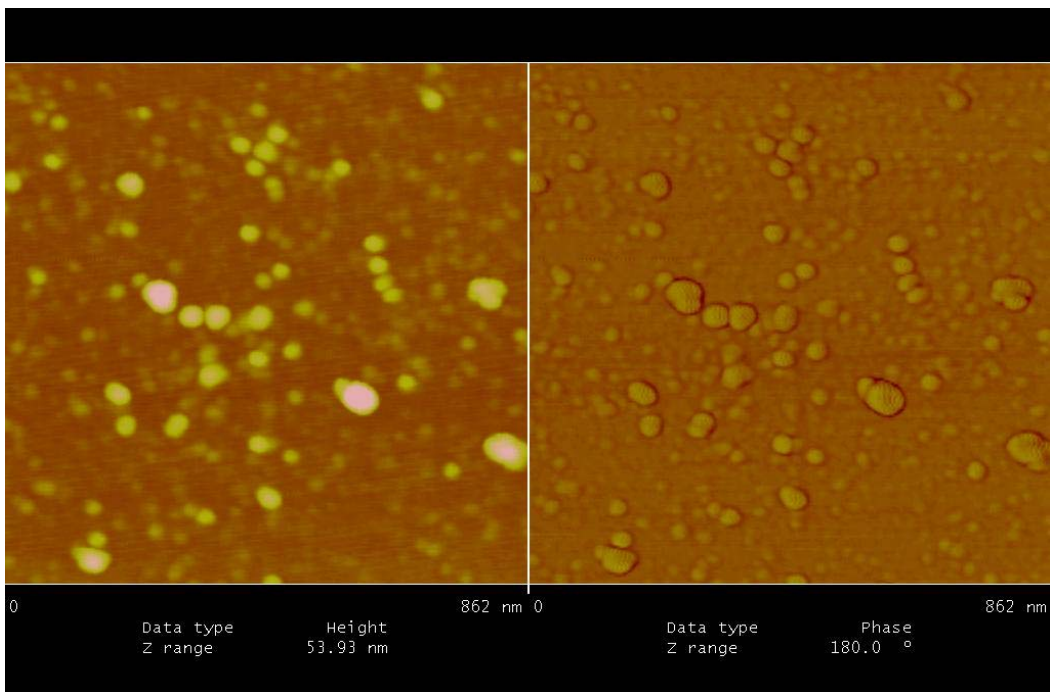


Figure 3-6. AFM topography (left) and phase (right) images of P3HT₄₁-*b*-PHEMA₈₂ sprayed from a THF/MeOH mixture (v/v = 1/99).

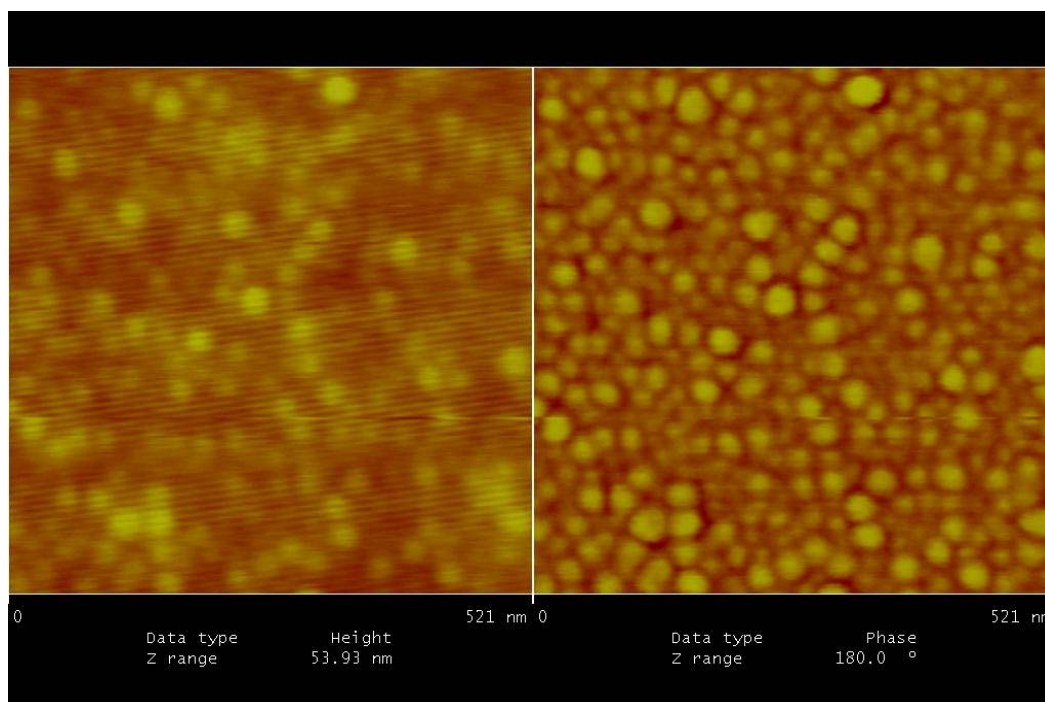


Figure 3-7. AFM topography (left) and phase (right) images of P3HT₅₃-*b*-PHEMA₆₀ sprayed from a THF/MeOH mixture (v/v = 1/99).

DLS was employed to analyze the polydispersity and hydrodynamic diameters (D_h) of the three P3HT-*b*-PHEMA diblock copolymers, in order to complement the morphological and topographical information obtained from the TEM and the AFM analyses. The results show that the average D_h values for the three P3HT-*b*-PHEMA block copolymer micelles were 33.0 ± 0.8 , 37.6 ± 0.5 , and 40.4 ± 1.2 nm (Table 3-2). These values are larger than diameters d_{TEM} and d_{AFM} , which were obtained from TEM and AFM, respectively. TEM probes probably only the diameters of the cores of the micelles, and AFM probes the overall diameters if the micelles. Meanwhile DLS experiments analyze the micelles in their solvated states. In a polar solvent environment, such as methanol, the corona of these particles swells, and increases the measured

diameter. The average polydispersities of these particles were also determined from DLS analyses. The polydispersity is the parameter to evaluate the size distribution of the particles, which is 0.12 for DC1, 0.09 for DC2, and 0.10 for DC3. The polydispersity data show that the micelles formed from the three P3HT-*b*-PHEMA block copolymers are systems with reasonable polydispersities.

3.3.2 UV-visible and Fluorescence Spectral Changes during Micelle Formation

Spectral properties were investigated in order to better understand how they are related to the self-assembly of the block copolymers. Similar to the morphology studies, the spectroscopic study of each P3HT-*b*-PHEMA sample was conducted by comparing samples prepared with different volume fractions. One sample of each was fully dissolved (with THF/MeOH, v/v = 94/6), while the other five THF/MeOH mixtures had higher methanol content (THF/MeOH, v/v = 70/30, 55/45, 40/60, 20/80, and 1/99) and were at various stages of micelle formation. Following this, comparison of the spectral properties among the three block copolymers was also conducted. Table 3-3 shows UV-visible absorbance (λ_{\max}) and fluorescence emission wavelengths (λ_{em}) of these samples before and after methanol addition.

Table 3-3. Spectral properties of P3HT-*b*-PHEMA samples.

Sample Name	Before Adding Methanol (THF/MeOH, v/v = 94/6)		After Complete Formation of Micelle (THF/MeOH, v/v = 1/99)	
	λ_{\max}	λ_{em}	λ'_{\max}	λ'_{em}
DC1	410	554	413	565
DC2	423	565	438	587
DC3	429	575	440	590

Figures 3-7 and 3-8 show the spectral analysis results of DC3 from the initial fully dissolved state (THF/MeOH, v/v = 94/6) to the final, complete micelle formation state (THF/MeOH, v/v = 1/99). The λ_{max} of the dissolved DC3 diblock copolymer in THF/MeOH (v/v = 94/6) is observed at 429 nm. As the methanol content increases, the absorption spectrum red-shifts slightly, and the λ_{max} shifts to 440 nm after the micelles have formed. Meanwhile, the absorbance decreases, due to the immobilization of the P3HT block, which aggregates at the micellar core. The corresponding fluorescence spectra of DC3 in THF/MeOH (v/v = 94/6) shows λ_{em} at 575 nm. As the methanol was added, the emission peaks gradually shifts from 575 to 590 nm, while the fluorescence intensity was also quenched as the micelles were formed. The red shift and the decreasing intensity in the fluorescence spectra reflect the possible interchain π - π stacking of the conjugated P3HT block in the sample DC3 in a THF/MeOH solvent mixture.¹⁰

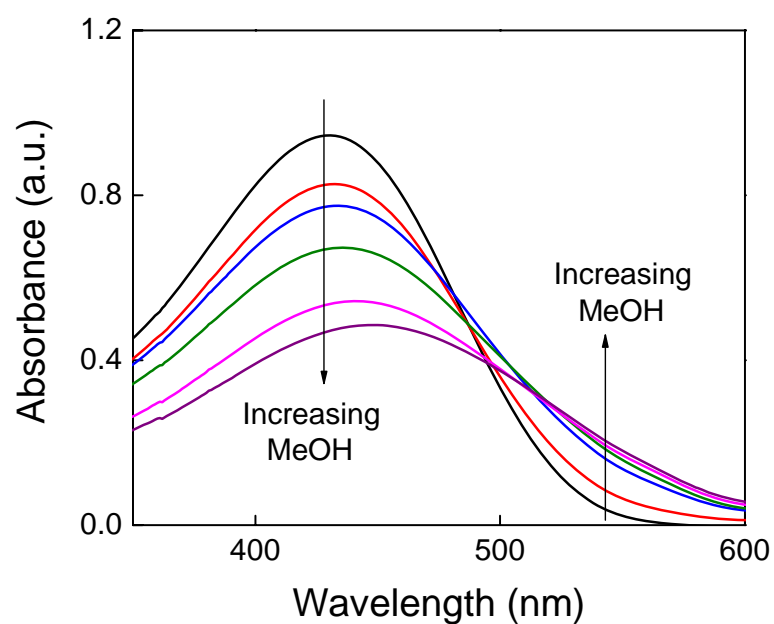


Figure 3-8. UV-visible spectra of DC3 in different solvent mixtures, with THF/MeOH volume fractions of 94/6, 70/30, 55/45, 40/60, 20/80, and 1/99.

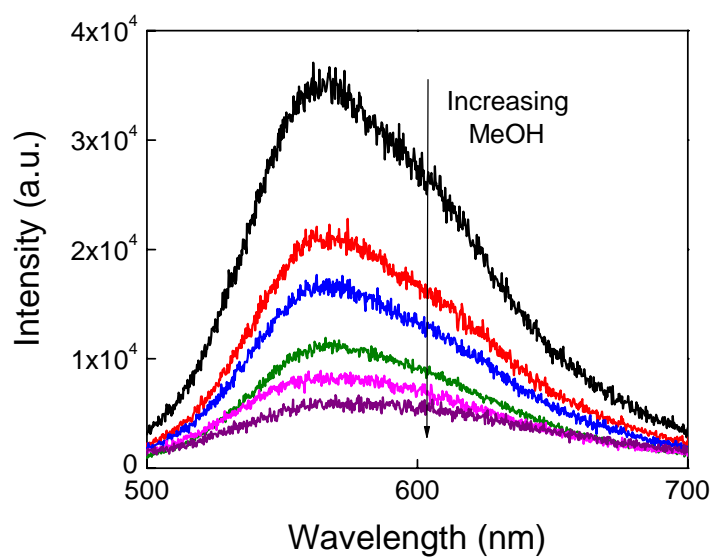


Figure 3-9. Fluorescence spectra of DC3 in different solvent mixtures with THF/MeOH volume fractions of 94/6, 70/30, 55/45, 40/60, 20/80, and 1/99.

The λ_{max} of DC1 and DC2 show similar red-shifts in the fully-formed micelle states (in THF/MeOH with v/v = 1/99), when compared to their fully-dissolved states (in THF/MeOH with v/v = 94/6). With increasing methanol content, the λ_{max} values of DC1 and DC2 shift from 410 to 413 nm, and from 423 to 438 nm, respectively (Figures 3-9 and 3-10). These two copolymers also showed a similar trend of decreasing absorbance intensity with increasing methanol content, as was observed with DC3. However, these decreases of absorbance intensities were smaller for DC1 (27%, from 0.749 to 0.546) and DC2 (41%, from 0.832 to 0.487), than for DC 3 (48%, from 0.945 to 0.489).

During the fluorescence experiments, when methanol was added to the samples, the emission peak (λ_{em}) of DC1 shifts from 554 nm to 565 nm, and λ_{em} of DC2 shifts from 565 nm to 587 nm (Figures 3-11 and 3-12). When the samples contained their highest methanol contents (with THF/MeOH, v/v = 1/99), the fluorescence intensities were finally quenched to their lowest values. This was possibly due to immobilization of the P3HT block, which had aggregated at the core of the micelle. For the micellar solutions of DC1 and DC2, the decreases of fluorescence intensities were 75% (from 3.85×10^4 to 9.5×10^3) and 90% (from 7.78×10^4 to 4.9×10^3).

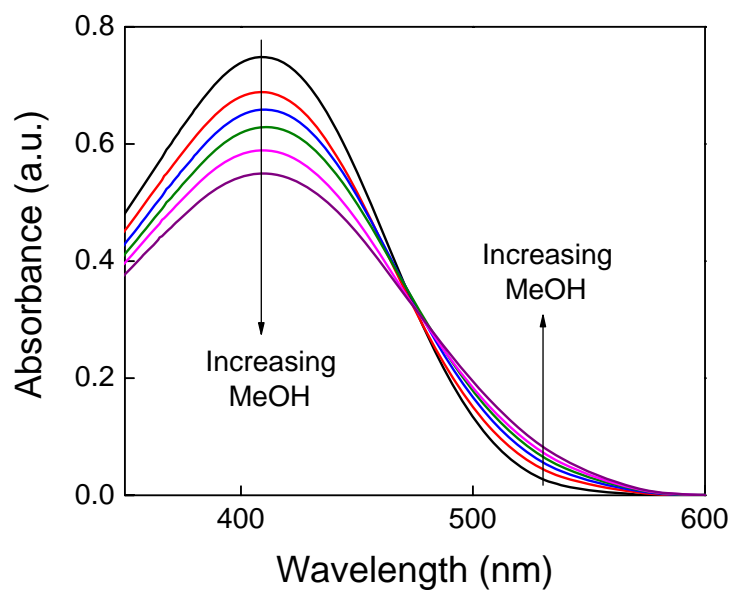


Figure 3-10. UV-visible spectra of DC1 with increasing methanol content during the micelle formation process (THF/MeOH, v/v = 94/6, 70/30, 55/45, 40/60, 20/80, and 1/99).

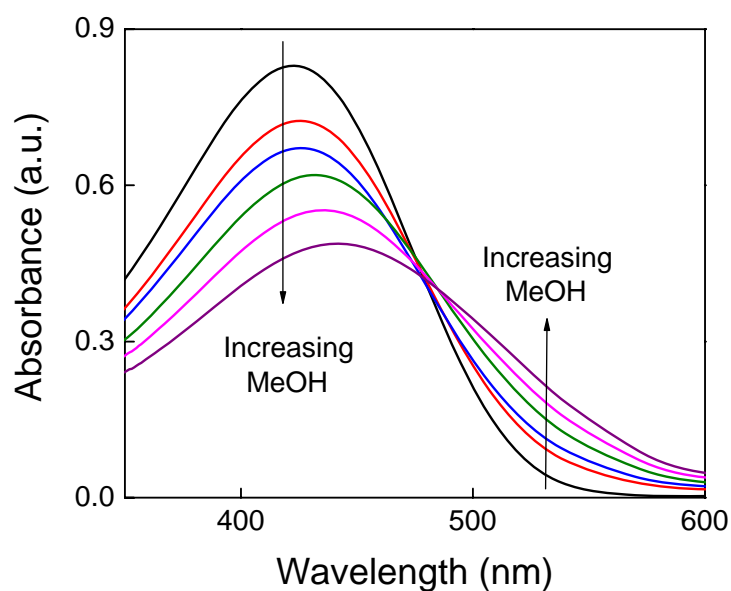


Figure 3-11. UV-visible spectra of DC2 with increasing methanol content during the micelle formation process (THF/MeOH, v/v = 94/6, 70/30, 55/45, 40/60, 20/80, and 1/99).

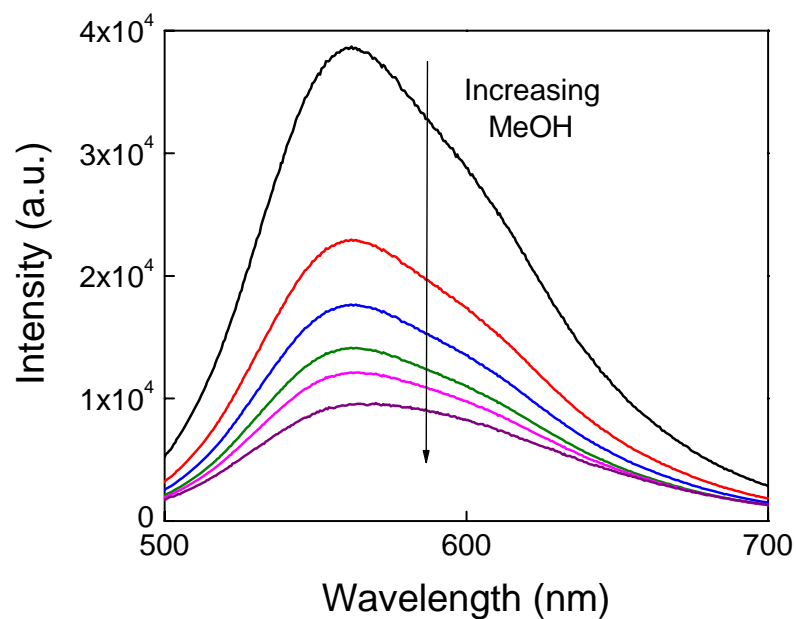


Figure 3-12. Fluorescence spectra of DC1 with increasing methanol content during the micelle formation process (THF/MeOH, v/v = 94/6, 70/30, 55/45, 40/60, 20/80, and 1/99).

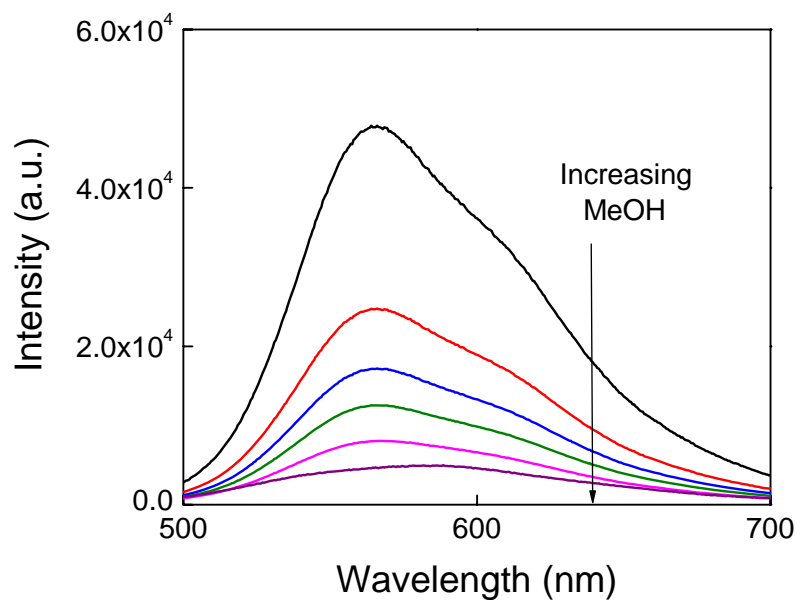


Figure 3-13. Fluorescence spectra of DC2 with increasing methanol content during the micelle formation process (THF/MeOH, v/v = 94/6, 70/30, 55/45, 40/60, 20/80, and 1/99).

3.4 Discussion for the Micelle Formation of the Diblock Copolymers

3.4.1 Factors Influencing the Sizes of Micelles

The morphological transition of the diblock copolymer in different THF/MeOH mixtures can be explained by the different interactions between the surface of the micelle and the solvent. By varying the content of the selective solvent, methanol, the quality of the solvent gradually becomes poorer for the P3HT block, which leads to increased interfacial tension between P3HT and the solvent. In order to counteract this energy increase, the micelle system itself must reduce the total interfacial area (per volume unit), which finally results in an increase in the micellar diameter. The length of the repeat unit within P3HT has been determined to be 0.39 nm.¹¹ This information could be used to determine approximate calculations of the length of the P3HT chains, and these calculated values appeared to be reasonable when compared with the TEM results (Table 3-4). AFM results showed that the aggregation of P3HT at the core of micelles was still not fully crystallized, because it was easily distorted by the tapping force. From the AFM image one can observe that there was a deformation, by comparing the larger diameters obtained by AFM with those that were obtained by TEM measurements.

Table 3-4. Comparison of the micelle diameters that were determined by TEM and AFM measurements with the calculated values.

Sample Name	P3HT repeat unit	d_{TEM} (nm)	d_{AFM} (nm)	$d_{\text{CALCULATION}}$ (nm)
DC1	30	10.1 ± 2.5	21.8 ± 6.7	11.7
DC2	41	14.9 ± 4.2	29.1 ± 9.3	16.0
DC3	53	18.7 ± 5.6	34.5 ± 6.1	20.7

In addition, the diameters of P3HT-*b*-PHEMA micelles increase with increasing P3HT block length. Therefore, the lengths of the P3HT and PHEMA blocks have an important effect on the micellar morphology. This can be explained by Vilgis theory.¹² For a given copolymer with a sufficiently large rod-to-coil ratio, the gradual deterioration of the solvent for the insoluble block leads to morphological transitions from spheres to cylinders and vesicles. The total free energy (F) of a micelle has three main contributions, which include the stretching energy of the coronal chains (F_n), the stretching energy of the core chains (F_r), and the interfacial energy between the core and the solvent (F_f). Because the coronal chain density is low, the contact is primarily between the core of the micelle and the solvent. The equations of the total free energy of these systems are given below:

$$F = F_n + F_r + F_f$$

$$F_r = \frac{4\pi r^2 \gamma_f}{f}, \text{ where } f \text{ is the chain packing number}$$

As the solvent deteriorates for the core block, γ_f increases. Hence in order to decrease F_r , the size of the core increases. This is counteracted by increases of F_n and F_f . Therefore, above a critical size, a particular morphology can become unsatable, and F is

minimized by a change of morphology.

For P3HT-*b*-PHEMA, longer PHEMA blocks give a larger contribution to the overall free energy. In order to avoid overcrowding, spherical, rather than cylindrical or vesicular, micelles tend to form. On the other hand, with an increase of the P3HT block, the folding number of P3HT increases, and thus the area occupied by each PHEMA chain becomes larger. This leads to a decrease in crowding of the tethered PHEMA block, and spherical micelles gradually increase their sizes as the length of the P3HT block increases.

3.4.2 Spectral Changes of the Micellar Solutions with Varying P3HT Volume Fraction

The relationship between the absorbance and emission spectral properties of these copolymers and their volume fraction of P3HT was also investigated. The volume fraction of P3HT was calculated by the following equation:

$$v_{\text{P3HT}} = \frac{M_{\text{P3HT}} / \rho_{\text{P3HT}}}{M_{\text{P3HT}} / \rho_{\text{P3HT}} + M_{\text{PHEMA}} / \rho_{\text{PHEMA}}}$$

where M_{P3HT} and M_{PHEMA} correspond to the molecular weights of the P3HT and PHEMA blocks, respectively. According to their repeat units, the densities of P3HT and PHEMA and $\rho_{\text{P3HT}} = 1.10 \text{ g/cm}^3$ and $\rho_{\text{PHEMA}} = 1.03 \text{ g/cm}^3$.^{13,14} Therefore the volume fractions of P3HT for DC1, DC2, and DC3 are 0.323, 0.387, and 0.528, respectively.

Since PHEMA lacks a chromophore, and does not absorb or emit light in the

UV-visible region, the UV-visible absorbance and fluorescence emission spectra observed were associated with the P3HT block. From Figures 3-13 and 3-14, it can be observed that both λ_{max} and λ_{em} increase as the P3HT volume fraction increases. It was expected that when the P3HT-*b*-PHEMA copolymers had formed micelles, that they would behave in a similar manner to the thin films of the P3HT homopolymer. This would be because when the P3HT block aggregates at the core of the micelle, it would be no longer dissolved in solution, but merely dispersed in the solvent. However, the changes in wavelength observed on going from the fully dissolved form to the micelle form of the P3HT-*b*-PHEMA block copolymer, were smaller than wavelength shifts observed between the solution and thin film spectra of the P3HT homopolymer. The UV-visible spectra of DC1 (which had 30 repeat units of P3HT), displayed a small λ_{max} shift from 410 to 413 nm when the copolymer was fully dissolved (THF/MeOH v/v = 94/6) and had completely formed micelles (THF/MeOH v/v = 1/99), respectively. Meanwhile, the spectra of the P3HT₃₃ homopolymer displayed a much larger shift, from 439 to 478 nm, for the solution and thin film spectra, respectively. Similar trends were observed for DC2 and DC3. This can likely be attributed to the aggregation of the P3HT block at the core of the micelle, where the P3HT becomes restricted to a confined volume, which results in twisting of the P3HT block. The wavelengths increase as the sizes of the micelles increase as observed by the λ_{max} values of 413 and 440 nm for DC1 and DC3, respectively. However, the λ_{max} values of these aggregated P3HT were still significantly shorter than those of the thin film of P3HT, where the chains of the P3HT homopolymers

have a greater chance to stretch and decrease the bandgap by extending the π -electron delocalization. Meanwhile, the apparent twisting of the P3HT block at the micelle cores is reflected by the d_{TEM} values, which are shorter than the calculated values (Table 3-4).

A similar trend was observed with the fluorescence emission wavelength, as the λ_{em} of each diblock copolymer increased with increasing volume fractions of P3HT (Figure 3-14). In addition, when this data was compared with that described in Chapter 2 (see Table 2-5), it became apparent that the red-shifts of the λ_{em} values corresponding to the aggregated P3HT at the cores of the micelles were smaller than those of the thin films. Also, the fluorescence intensities of each of the three diblock copolymers were plotted against the methanol volume fraction. For these samples, a large reduction of their fluorescence intensities were observed from the starting points (THF/MeOH, v/v = 94/6), to the second mixtures (THF/MeOH, v/v = 70/30), as shown in Figure 3-15. Beyond this point, their fluorescence intensities also continued to decrease, although less dramatically, as more methanol was added. It appears that the fluorescence was quenched at the beginning of the micelle formation process, as further additions of methanol to the micellar solutions resulted smaller decreases of the fluorescence intensities compared to the initial addition.

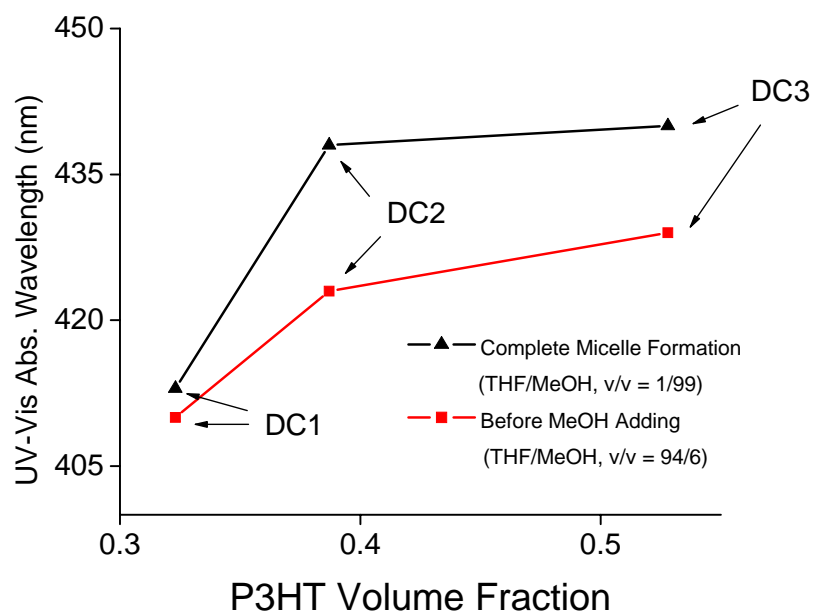


Figure 3-14. Plot of the UV-visible maximum absorption wavelength (λ_{\max}) against the P3HT volume fraction before and after methanol addition.

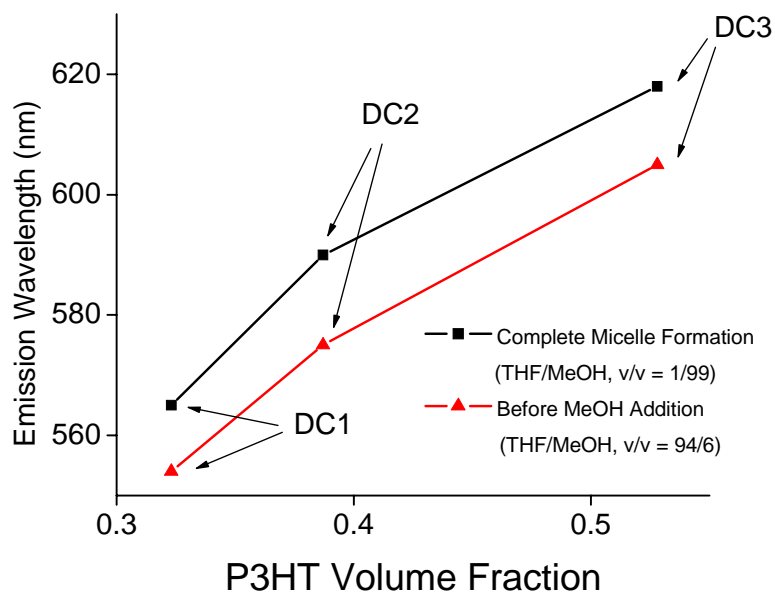


Figure 3-15. Plot of the fluorescence emission wavelength (λ_{em}) against the P3HT volume ratio before and after methanol addition.

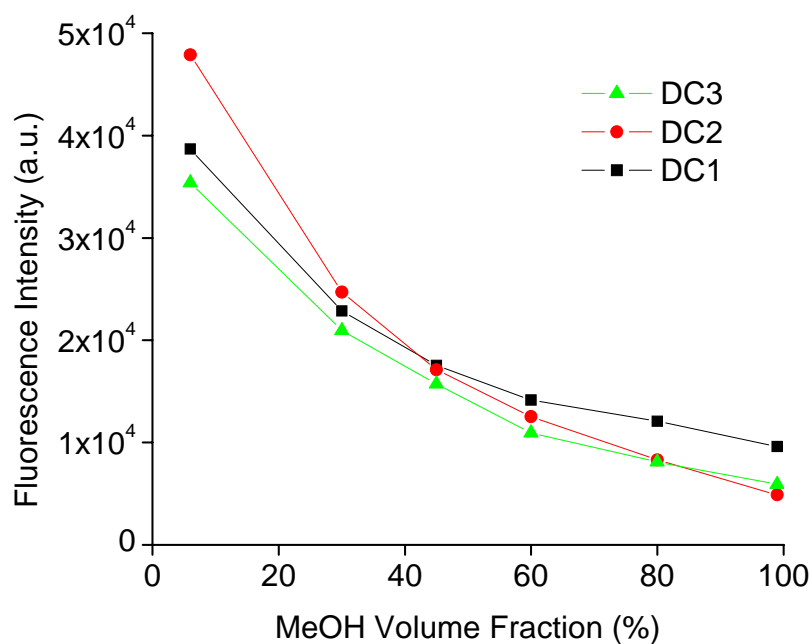


Figure 3-16. Plot of the fluorescence intensity against the methanol volume fraction, in THF/MeOH solvent mixtures during the micellar preparation process.

3.5 Conclusions

In this chapter, the morphological and spectral properties of rod-coil diblock copolymers of P3HT-*b*-PHEMA were investigated. They were characterized by TEM, AFM, DLS, UV-visible and fluorescence spectrometry. These methods allow a further understanding of micellar morphologies and how they are formed in a selective solvent.

It was found that the differences of the diblock lengths were reflected by the morphologies of the micellar aggregates formed in the THF/MeOH solvent mixtures. This study highlights the importance of the effect that polymer composition has on the aggregated structures of rod-coil diblock copolymers in dilute solution. The diameters

of the micelles, and the absorption and emission wavelengths increased as the length of the length of the P3HT block increased. Furthermore, it was found that the spectral properties of the P3HT-*b*-PHEMA micelles are related to the P3HT volume fraction. This is an important factor which determines the stacking of the P3HT block at the cores of the micelles. Knowing this, the number of repeat units within the P3HT block can be adjusted to influence the spectral properties of the polymer, and potentially aid in the design and development of photovoltaic devices.

References

- 1 Jenekhe, S. A. Chen, X. L. *Science* **1998**, 279, 1903.
- 2 Leclere, P. Calderone, A. Marsitzky, D. Francke, V. Geerts, Y. Mullen, K. Bredas, J. L. Lazzaroni, R. *Adv. Mater.* **2000**, 12, 1042.
- 3 Sommer, M.; Lang, A. S.; Thelakkat, M.; *Angew. Chem. Int. Ed.* **2008**, 47, 7901-7904.
- 4 Iovu, M. C.; Zhang, R.; Cooper, J. R.; Smilgies, D. M.; Javier, A. E.; Sheina, E. E.; Kowalewski, T.; McCullough, R. D. *Macromol. Rapid Commun.* **2007**, 28, 1816-1824.
- 5 Dai, C.-A.; Yen, W.-C.; Lee, Y.-H.; Ho, C. C.; Su, W.-F. *J. Am. Chem. Soc.*, **2007**, 129, 11036-11038.
- 6 Higashihara, T.; Ohshimizu, K.; Hirao, A.; Ueda, M. *Macromolecules*, **2008**, 41, 9505-9507.
- 7 Sauv e, G.; McCullough, R. D. *Adv. Mater.* **2007**, 19, 1822-1825.
- 8 Zhou, Z.; Chen, X.; Holdcroft S. *J. Am. Chem. Soc.*, **2008**, 130, 11711-11718.
- 9 Chen, X.; Gholamkhash, B.; Han, X.; Vamvounis, G.; Holdcroft, S. *Macromol. Rapid Commun.* **2007**, 28, 1792-1797.
- 10 Lin, C.-H.; Tung, Y.-C.; Ruokolainen, J.; Mezzenga, R.; Chen, W.-C.; *Macromolecules* **2008**, 41, 8759-8769.
- 11 Yang, X.; Loos, J.; Veenstra, S. C.; Verhees, W. J. H.; Wienk, M. M.; Kroon, J. M.; Michels, M. A. J.; Janssen, R. A. J. *Nano Lett.* **2005**, 5, 579-583.
- 12 Vilgis, T.; Halperin, A.; *Macromolecules* **1991**, 24, 2090.
- 13 Mardalen, J.; Samuelsen, E. J.; Gautun, O. R.; Carlsen, P. H. *Solid State Commun.* **1991**, 77, 337.
- 14 Eschbach, F. O.; Huang, S. J. *J. Bioact. Compat. Polym.* **1994**, 9, 51.

Chapter 4. Summary

4.1 Molecular Weight Dependence of P3HT

Regioregular P3HT polymers with a narrow molecular weight distribution ($PDI < 1.25$) were studied. A key point discovered in this study was the influence of the molecular weight of P3HT on its physical and spectral properties. The information has not been revealed previously, as most studies have focused on high molecular weight P3HT ($> 150,000$ g/mol) and have neglected the fundamental properties of low molecular weight P3HT ($< 15,000$ g/mol). Due to the high regioregularities (90% ~ 95%) and narrow molecular weight distribution ($PDI < 1.25$) of the polymer samples prepared in the study, the pristine properties of molecular weight dependence of P3HT were revealed, and deviations due to variations of the regioregularity of the polymer chain were minimized. The refractive index increment, the maximum absorption wavelength, the emission wavelength, and the extinction coefficient were found to increase with increasing molecular weight. The figures in Chapter 2 present this ascending trend for these relations. Moreover, when the number of repeat units of the P3HT backbone surpasses 45, these optical and spectral properties begin to approach asymptotic values.

4.2 Micellar Morphology of P3HT-*b*-PHEMA block copolymers

Diblock copolymers P3HT-*b*-PHEMA were studied after the polymerization of HEMA units onto a P3HT block. These novel rod-coil block copolymers (with P3HT acting as the rod and PHEMA acting as the coil) were used in order to understand how micellar aggregates containing one conductive polymer block formed in a selective solvent. As with the studies of the P3HT homopolymer, the techniques of TEM, AFM, DLS, UV-visible, and fluorescence spectrometry were used to characterize the morphological and spectral properties of the P3HT-*b*-PHEMA block copolymers. In this study, three P3HT-*b*-PHEMAs block copolymers, each with a different number of repeat units, were compared by their micelle size, UV-visible absorbance, and fluorescence emission properties. It was found that the maximum absorbance and emission wavelengths increase as the volume fraction of P3HT block of the P3HT-*b*-PHEMA copolymer increased. Due to the incorporation of the PHEMA block with these diblock copolymers, the UV-visible and fluorescence spectra of these copolymers did not shift as significantly as those of the P3HT homopolymers with similar numbers of repeat units.

4.3 Significance of Work

Regioregular P3HT has attracted attention because of its good stability, conductivity, and solubility in organic solvents. However, limitations still exist, as only a limited variety of organic solvents can be used to fabricate P3HT. Thus, the

incorporation of functional groups into the P3HT is considered as one possible way to improve its solubility in a variety of other solvents. Successful functionalization was believed to allow P3HT to be dissolved in polar solvent systems, such as methanol. In addition, a better understanding of the novel P3HT-*b*-PHEMA block copolymers can aid in the comprehension of the relationship between its morphological and spectral properties. This would allow the building of more complex nanostructures from rod-coil block copolymer micelles, and for the application of P3HT as a chemical sensor, where its adsorption properties could be used to detect changes in environment.

4.4 Future Work

Future work will focus on the exploration of the micellar and the bulk phase morphologies of other P3HT-containing block copolymers, such as and P3HT-*b*-P(HEMA-C₆₀) copolymers. Films will be produced on indium tin oxide (ITO) glass, and it is expected that self-aggregated bulk-heterojunction structures will form. Several methods will be used to study these films, including X-ray diffraction, TEM, AFM, and *I-V* characterization. The further exploration of these projects will lead to a comprehensive understanding of the mechanism of the electron and energy transfer process for block copolymers containing a conductive P3HT block.